INFORMATION TO USERS

This manuscript has been reproduced from the microfilm master. UMI films the text directly from the original or copy submitted. Thus, some thesis and dissertation copies are in typewriter face, while others may be from any type of computer printer.

The quality of this reproduction is dependent upon the quality of the copy submitted. Broken or indistinct print, colored or poor quality illustrations and photographs, print bleedthrough, substandard margins, and improper alignment can adversely affect reproduction.

In the unlikely event that the author did not send UMI a complete manuscript and there are missing pages, these will be noted. Also, if unauthorized copyright material had to be removed, a note will indicate the deletion.

Oversize materials (e.g., maps, drawings, charts) are reproduced by sectioning the original, beginning at the upper left-hand corner and continuing from left to right in equal sections with small overlaps.

Photographs included in the original manuscript have been reproduced xerographically in this copy. Higher quality 6" x 9" black and white photographic prints are available for any photographs or illustrations appearing in this copy for an additional charge. Contact UMI directly to order.

UMI®

Bell & Howell Information and Learning
300 North Zeeb Road, Ann Arbor, MI 48106-1346 USA
800-521-0600

Equating Discriminability of Subjective Contours Across the Visual Field Requires Two Scaling Factors

Frédéric J. A. M. Poirier

A Thesis

in

The Department

of

Psychology

Presented in Partial Fulfillment of the Requirements

for the Degree of Master of Arts at

Concordia University

Montréal, Québec, Canada

August, 1997

ABSTRACT

Equating Discriminability of Subjective Contours Across the Visual Field Requires Two Scaling Factors

Frédéric J. A. M. Poirier

Performance in visual tasks can often be equated across eccentricities by proper scaling. The scaling or inverse magnification function (IMF), describes the ratio of peripheral to foveal stimulus size required to equate performance. Tasks and visual brain regions have different IMFs. It is argued in this thesis that IMFs may average out when a methodology insensitive to the presence of multiple IMFs is used. This fact is demonstrated through simulations. The present thesis introduces a data fitting technique that detects the presence of multiple IMFs in a psychophysical task. These are revealed as an interaction between stimulus configuration and eccentricity. These new techniques were used to investigate the percept of subjective contours (SC) defined by offset gratings which are thought to be encoded through a cooperation of V1 and V2 cells, two brain areas described by different IMFs. Five participants discriminated the orientation of a SC presented foveally (monocularly or binocularly) and at four eccentricities. SC length and carrier grating wavelength were adjusted until performance converged on 81% correct. There was an interaction between eccentricity and stimulus configuration, $F(20, 80) = 2.063$, $p = .0124$, which was accounted for only if two IMFs were assumed. It was found that SC length (V2) scaled faster than the wavelength (V1) as a function of eccentricity. This qualitatively agrees with anatomical measures of V1 and V2 IMFs. The method developed here provides a more informative and more objective measure of eccentricity-dependent performance limitations than other commonly-used methods.

Acknowledgements

I gratefully acknowledge the guidance and many insightful ideas of Rick Gurnsey (research supervisor), and the help of Peter April (department programmer) for making this research possible. I also would like to thank the participants for their patience and time commitment. Finally, I thank Julia Savina, Danuta Rajska and Bruno Lombardi for moral support and proofreading. This research was supported partially with NSERC grants.

Table of Contents

List of Figures

List of Tables

List of Equations

Many animals have evolved complex visual systems which permit the detection and recognition of objects such as food or predators from large distances. It is not surprising given the importance of vision that "over half of the neocortex in nonhuman primates is occupied by visual areas" (Sereno et al., 1995, p.889). Image contours provide critical information for image segmentation. Contours define the position and shape of objects, and serve as a first step in the processing of visual information. Contours may be defined by a multitude of characteristics such as luminance, color, contrast, motion, binocular disparity and texture. However, the recovery of contours may require several steps of processing.

The recovery of contours depends on acuity limits. Acuity is better when stimuli are presented in the foveal region of the retina rather than in the peripheral region. This is not surprising because the density of photoreceptors is greater in the foveal region. The oversampling of the foveal region is a general feature of many visual areas in the brain. The present thesis examines the visual system's ability to recover contours defined by shifted gratings for presentations across a wide range of eccentricities.

Anatomical Hierarchy of Stages

Precortical Areas. Visual information is encoded by the brain in series of processing stages. Figure 1 depicts the anatomical hierarchy of visually responsive brain regions from retina, LGN, V1, V2 and then to higher cortical areas. Each region is associated with a selectivity for a different kind of spatial stimuli. Light falling on the retina is absorbed by rods and cones. Electro-chemical signals from the rods and cones are collected by retinal ganglion cells in a restricted region of the retina, thus forming a receptive field. "A

neuron's receptive field is the area on the receptor surface (the retina[...]) that, when stimulated, affects the firing of that neuron." (Goldstein, 1996, p. 614). Many retinal ganglion cells and LGN cells fire vigourously when the intensity of light presented to the center of the receptive field differs from that presented to the surrounding region (Bradley, Skottun, Ohzawa, Sclar & Freeman, 1985; 1987). Such an antagonistic center-surround arrangement is particularly sensitive to luminance discontinuities in the stimulus irrespective of the retinal orientation of the discontinuity. These transformed signals are then relayed to the primary visual cortex (V1).

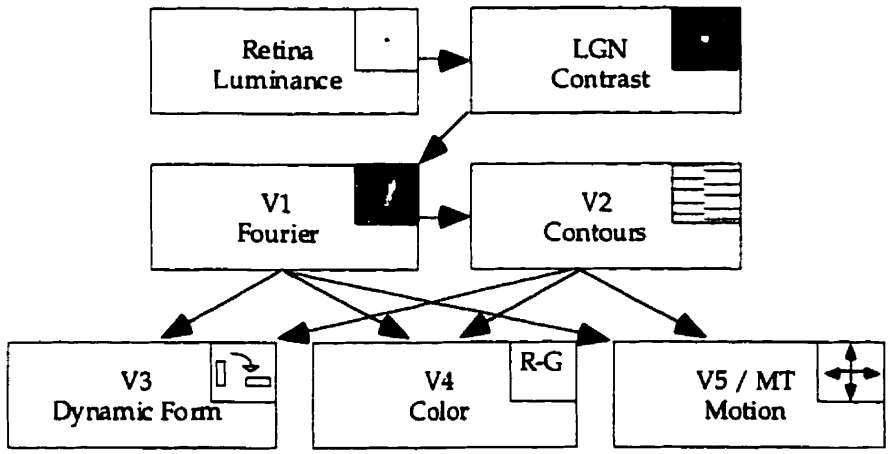

Figure 1. Structures from retina to cortex. Arrows depict the major bottom-up connections between visual areas. As signals progress from lower levels (retina and LGN) to higher levels (V3, V4 and V5), cells respond to increasingly complex stimuli (as shown in boxes). For example, cones in the retina respond according to the quantity of light present, retinal ganglion cells respond to nonoriented discontinuities in retinal luminance, V1 simple cells respond to oriented changes in retinal illumination and V2 "contour" cells respond to more abstract orientation structures.

Area V1. Area V1 receives signals from the LGN. Although V1 exhibits ocular dominance (Hubel, Wiesel & Stryker, 1978; Hubel & Wiesel, 1974a; 1974b) and selectivity for direction and stereoscopic disparity (DeAngelis, Ohzawa & Freeman, 1991), *orientation* and *spatial frequency* selectivity are critical features of many cells in V1 with respect to the recovery of spatial form (Hubel et al., 1978; Hubel & Wiesel, 1974a; 1974b; DeValois, Albrecht, &

Thorell, 1982). Simple cells have inhibitory and excitory regions in their receptive fields. A consequence of this is that oriented structures must be precisely positioned within the cell's receptive field to elicit optimal responses. Complex cells, on the other hand, respond homogenously to stimulation across their receptive field, i.e. complex cells showing orientation selectivity do not require precise positioning. A characteristic of V1 and many other visual areas is that cells having the same stimulus preference will be arranged in columns perpendicular to the surface. For example, cells preferring lines oriented at 10° are aligned in columns. The same is true for ocular dominance (Hubel & Wiesel, 1974a) and spatial frequency (DeValois et al., 1982).

Simple cells in V1 are both orientation- and wavelength-selective (Hubel & Wiesel, 1974a; 1974b; DeValois et al., 1982). The wavelength of a sine-wave grating is the distance between two consecutive luminance peaks (in degrees of visual angle per cycle), which is the inverse of the spatial frequency (in cycles per degree of visual angle). The term wavelength will henceforth be used. The right panel of Figure 2 shows the response of a simple cell to sine wave gratings of constant contrast but of different wavelengths. Such a "tuning curve" shows a peak response at the preferred wavelength and responses fall off on either side of this peak. The left panel of Figure 2 shows that a similar pattern of responses occurs when the cell is stimulated with sine wave gratings of different orientations. Wavelength columns (DeValois et al., 1982) comprise cells processing an area of the visual field for a range of wavelengths. However, this column has limits both in the higher and lower range of wavelengths (see Wilson, Levi, Maffei, Rovamo & DeValois, 1990); wavelengths above a certain point don't give rise to a neural signal and those below a certain point give rise to an erroneous

representation called "aliasing" (see Thibos, Still & Bradley, 1995) or are blurred by the optics.

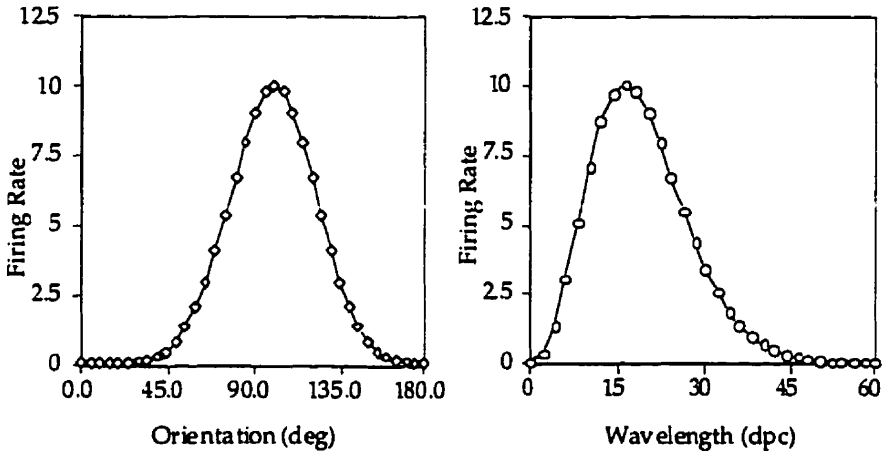

Figure 2. Orientation and wavelength selectivity of V1 simple cells. As can be seen, simple cells prefer stimuli that are of a given orientation (left) and wavelength (right) but will not respond to similar stimuli if presented at a different orientation or wavelength. Similar cells exist for each orientation and a large range of wavelengths.

Area V2. Area V2 receives most of its input from area V1. V2 is believed to perform a higher-order analysis of the visual stimuli. For example, many cells in V2 respond to abrupt phase changes in a line grating (see Figure 4A) for which the average luminance is the same on both sides of the boundary (von der Heydt, Peterhans, & Baumgartner, 1984). In contrast, V1 cells respond only to luminance changes between two regions and would not respond to a phase-defined boundary. The response of V2 contour cells are relatively invariant to the characteristics of the carrier (i.e. the grating used to build the SC) but are tuned to the characteristics of the SC (its position and orientation). It will be shown later that pooling the responses of V1 cells across a range of wavelengths and orientations would enable V2 cells to respond to "second order" changes in the stimulus, as exemplified by SCs and more generally by texture boundaries. It is interesting to note that many SC

cells in V2 also respond to a simple luminance contour.

Eccentricity

Anatomy. Many studies have shown that cones are more densely packed in the foveal region of the retina than in the peripheral regions (Hirsch & Curcio, 1989; Rolls & Cowey, 1970). As well, from fovea to periphery there is a greater convergence of cones onto retinal ganglion cells, i.e. there is an increase in the size of the retinal region processed by a retinal ganglion cell from fovea to periphery. Similarly, the retinal area processed by a unit area of cortex changes as a function of eccentricity from the fovea (Sereno et al., 1995; Hubel & Wiesel, 1974b). A magnification function (MF) "indicates how much cortical [length] represents a unit of visual field at different eccentricities" (Mulligan & Sherk, 1993, p.195). A simple MF often used is:

$$M = 1 / (1 + E / E_2), \qquad \text{[Eq 1]}$$

where E is the eccentricity of presentation (from fovea) and E_2 is the distance from the fovea (in degrees of visual angle) where the cortical magnification is half of that found at the fovea (see Figure 3). Therefore, M is the ratio of the number of peripheral to foveal cells stimulated by a pattern of fixed size. Inverse magnification functions (IMF) specify the sizes of visual stimuli required to stimulate a constant number of cells at each eccentricity (see Figure 3). An often used IMF is Equation 2, which is a simple reformulation of Equation 1:

$$M^{-1} = 1 + E / E_2, \qquad \text{[Eq 2]}$$

By definition, E_2 is the eccentricity at which a stimulus twice the foveal stimulus size ($M^{-1} = 2$) that will stimulate the same number of cells. E_2 is *inversely proportional* to the *rate* at which stimulus size must change with eccentricity in order to maintain stimulation of a constant number of cells. Equations 1 and 2 are depicted in Figure 3. In addition to being well-suited to describe cortical magnification in visual areas, these equations are also used to describe other physiological changes with eccentricity. For example, Equation 1 has been used to describe cone density changes and Equation 2 has been used to describe eccentricity-dependent changes in receptive field size. It should be noted that many if not most psychological and physiological IMFs are well-described by a linear function, as probably first observed by Weymouth (1958). However, the precision of the IMF is highly dependent on the precision of the foveal value because magnification factors are expressed relative to the foveal value.

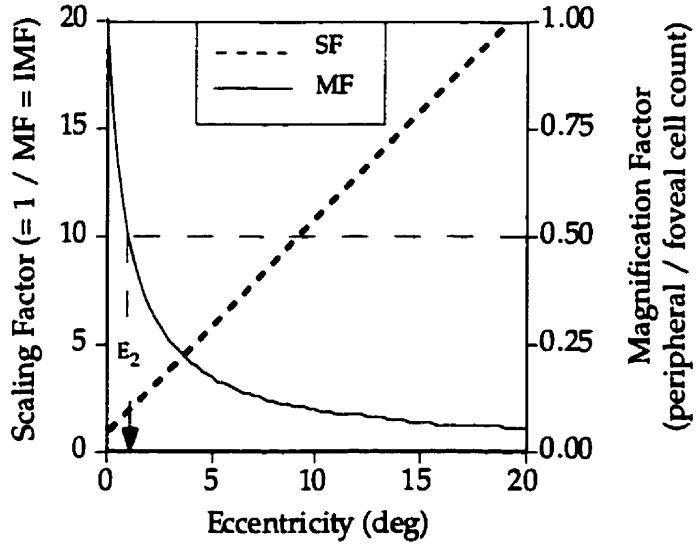

Figure 3. MFs and IMFs. The number of cells processing a unit visual area is eccentricity dependent. This phenomenon is called "magnification" which refers to the fact that foveal representations are cortically magnified relative to peripheral stimuli. The magnification function (MF) describes the change of magnification as a function of eccentricity (continuous line). When stimuli are created so as to stimulate the same number of cells at each eccentricity

of presentation, the function relating stimulus size and eccentricity of presentation is linear (dotted line). This function, which is the reverse of the MF, is referred to as inverse magnification function (IMF) or scaling function (SF).

Different visual areas have different IMFs. From the retina to V2, each successive stage puts more emphasis on foveal presentations than the previous one, which is reflected by smaller E_2s (Wilson et al., 1990; Hirsch & Curcio, 1989; Sereno et al., 1995). Because each successive stage takes its input primarily from the previous one (Smith, Chino, Ridder, Kitagawa & Langston, 1990; Mulligan & Sherk, 1993; Hubel, 1996), it logically follows that a given stage has more connections with the foveal region of the preceding stage than with the peripheral region. Given that higher cortical areas are specialized in processing higher-order information in the stimulus, it seems beneficial to process simple features across the visual field in lower areas yet to preferentially process complex integrations mostly foveally in higher areas.

Psychophysics. Many psychophysical results can be understood in terms of these IMFs. On the assumption that physiological changes are compensated for by equivalent changes in stimulus size (see Equation 2), then performance can be made independent of eccentricity by scaling the stimuli appropriately. By finding the stimulus size at each eccentricity that elicits performance equal to that of the fovea, the IMF can be determined and E_2 calculated. IMFs are often referred to as "scaling functions" because they describe the scale of a stimulus that equates performance at each eccentricity. This IMF or scaling function may then be related to known physiological changes in the density of photoreceptors, receptive field sizes, or cortical magnification.

This concept is well illustrated by a grating acuity task, in which a grating (either square-wave or sine-wave) is reduced in wavelength until individual lines cannot be resolved. As one would expect, the minimum

wavelength resolveable increases with eccentricity (Rovamo & Virsu, 1979; Virsu, Näsänen & Osmoviita, 1987; Thibos et al., 1996). An IMF with an E_2 between 2.38 and 4.14 provides a good fit to grating acuity tasks (see Table 1 for a review of grating acuity and their E_2 values). This E_2 also characterises changes in retinal ganglion cell density with eccentricity (Rovamo & Virsu, 1979). It can therefore be suggested that grating acuity is dependent upon the spacing of retinal ganglion cells.

One IMF per Task. In general, IMFs seem to be task specific, or, more precisely, to depend on that dimension of the stimulus which limits performance. For example, unreferenced movement acuity (detecting motion of a dot without any other points of reference) is usually less affected by eccentricity of presentation than bisection acuity (judging the mid-point of a gap between two dots). Indeed, the E_2s for these two tasks differ by a factor of more than 100 (Whitaker, Mäkelä, Rovamo, & Latham, 1992). This qualitatively parallels the IMFs of the "motion" (magnocellular) and "form" (parvocellular) pathways (e.g. Ungerleider & Mishkin, 1982) at least below and at V2 (Baseler & Sutter, 1997; see Wilson et al., 1990 for review, but see Whitaker, Mäkelä et al., 1992). On the other hand, many sources of limitations may be reflected in the results of a particular psychophysical task. That is, for a form discrimination task, both retinal and cortical limitations may combine to limit performance in a simple task. For example, loss of performance due to cone density is not equivalent to loss of performance due to the limitations of the cortical magnifications because cone density decreases at a slower rate than either the V1 or V2 cortical magnifications (Wilson et al., 1990; Morrone, Burr, & Spinelli, 1989; Virsu et al., 1987).

One IMF per Visual Area. The change of IMFs from one visual area to the next has led several researchers to believe that the IMF associated with a

particular task could help to determine the visual area that limits performance in the task. For example, Yu and Essock (1996) measured the facilitatory and inhibitory regions associated with a line-detection task. In their study, a small background either elevated or reduced line-detection thresholds. When the extent of the background is increased, thresholds first increase and then decrease to an asymptotic level. The dependence of threshold on background extent has been modeled by end-stopped mechanisms (such as found in V1; DeAngelis, Freeman, & Ohzawa, 1994; Orban, Kato, & Bishop, 1979) that prefer lines of a certain *length* as well as particular width. Yu and Essock (1996) measured the dimensions of the central excitatory region, the flanking regions and the end-stopped regions at eccentricities of 0°, 5°, and 10°. They found that each of the three subregions of the end-stopped mechanism required a different E_2. On the basis of the derived E_2s, they classified the end-stopped cells' center, flank and end regions as being limited by retinal, LGN and cortical mechanisms respectively (discussed in detail in the Discussion under "End-Stopped Cells").

Eccentricity-Dependent Limits on Spatial Vision. Table 1 presents a summary of relevant research in the field of magnification and psychophysical changes with eccentricity. The classification is a combination of several previously published tables and of other relevant studies (see Wilson et al., 1990; and Rovamo, Mäkelä, Näsänen & Whitaker, 1997 for reviews). From left to right the columns present (1) the type of psychophysical task or the physiological structure (denoted by •) that was investigated, (2) the E_2s derived, (3) the foveal value (i.e. minimum foveal size required to perform task or foveal cell density) and (4) the reference. In several cases, an estimation (or re-estimation) of E_2 and of the foveal threshold size was required. Estimations, denoted by the symbol ≈, were done by linear fitting of

the data when available or by interpolation from the graphs. A † sign indicates that the researchers considered the presence of multiple E_2s within the task. The tasks or structures have been ordered to reflect plausible commonalities between the psychophysical results and the proposed physiology.

In general, it appears from Table 1 that tasks using positional cues such as relative position of the elements (e.g. bisection acuity) are associated with smaller E_2s (Levi et al., 1985). Similarly, higher-order visual areas are also associated with smaller E_2s. This suggests that the mechanisms responsible for static stimuli and hyperacuities are in greater concentration in the foveal region while mechanisms detecting changes or presence of simple stimuli are more evenly spread across the retina. This is well illustrated in the results of Thibos et al. (1996). They compared a detection task (presence vs absence of a grating) and a discrimination task (vertical or horizontal orientation of the grating; called grating resolution in Table 1). They found that grating detection was much better in the periphery than its resolution (grating discrimination). Hence, the simpler task of "detecting" the grating was associated with a larger E_2 (85.1° for detection[1] vs 4.14° for resolution).

[1]Detection was reevaluated without the foveal value because the foveal detection curve seems to be determined by the resolution of the grating. Linear fit was used to find the E_2 and the foveal intercept.

Table 1: Magnification in Physiology and Behavior

Task / Structure	E2	Fov. Min.	Reference(s)
Grating Detection	≈85.1	≈120"	†Thibos et al., 1996
Unreferenced Motion	6.3 to 18.5	≈500"	Whitaker, Mäkelä et al., 1992
•Monkey RF Size	≈5.82		Hubel & Wiesel, 1974b
Line / Spot Detection	3.79-5.49		†Yu & Essock, 1996
End-Stopped: Center	2.05	11' x 6'	†Yu & Essock, 1996
T: Up vs Down	2.04±.19	≈1'	†Toet & Levi, 1992
Contrast Sensitivity	≈2.00 to 4.54		Morrone et al., 1989; Watson, 1987; Rovamo, Virsu & Näsänen, 1978
•RGC Density	≈2.38 to ≈3.45	7.51'/mm	Rovamo & Virsu, 1979
Grating Resolution	≈2.38 to ≈4.14	38" to 2'	Rovamo & Virsu, 1979; Virsu et al., 1987 †Thibos et al., 1996
•Monkey V1 MF	≈1.97		Hubel & Wiesel, 1974b
Orientation	.77 to ≈5.82		Scobey, 1982; Paradiso & Carney, 1988 Poirier & Gurnsey, 1996, submitted
	1.95	1.49'	Mäkelä, Whitaker & Rovamo, 1993
Vernier Acuity	1.51 to ≈3.45		Whitaker, Rovamo, MacVeigh & Mäkelä, 1992; Virsu et al., 1987; Westheimer, 1982
•Human V1 MF	1.237	4.38'/mm	Grüsser, 1995
•Human V1 MF	0.75	2.60'/mm	Horton & Hoyt, 1991
End-Stopped: Flanks	.77	6'-8'	†Yu & Essock, 1996
End-Stopped: End	.45	9'	†Yu & Essock, 1996
T: Interference			
Tangential	.34±.04	≈6'	†Toet & Levi, 1992
Radial	.18±.03	≈6'	†Toet & Levi, 1992
Spatial Interval	.07 to .22		Whitaker, Mäkelä et al., 1992
Bisection Acuity	.07 to .08	≈.3 to ≈.4'	Whitaker, Mäkelä et al., 1992

Problems with the Methods Used to Study the IMFs

Recent research points to the fact that many studies using magnification suffer from several problems.

(1) Prescaling. Many studies choose a IMF and scale their stimuli

accordingly in order to reduce eccentricity-dependent variability. Unless the goal of the research is primarily to investigate other phenomena (Poirier & Gurnsey, 1996, submitted; Carrasco & Frieder, 1997), this strategy can't recover the IMF hence isn't useful to investigate eccentricity-dependent changes in performance. Scaling the display using predetermined IMFs is considerably less sensitive to eccentricity-dependent performance changes than determining the size at each eccentricity required to equate performance. As can be seen using IMFs based on theoretical assumptions, E_2s in an orientation task can vary from .77 to ≈5.82 and still apparently compensate for all eccentricity-dependent variability in the data (see Table 1) (Paradiso & Carney, 1988; Scobey, 1982). These results would probably agree better if the E_2s would have been calculated (Mäkelä et al., 1993). It is therefore recommended that E_2 be measured rather than assumed.

(2) Terminology. Many terms are used imprecisely by psychophysicists. For example, "cortical magnification" is a term used by physiologists to refer to the area of cortex stimulated by a pattern of fixed size at various eccentricities. However, the term cortical magnification has been (wrongly) used to designate changes in retinal ganglion cell density (from Rovamo et al., 1978; see Rovamo et al., 1978; Rovamo & Virsu, 1979; Virsu, Rovamo, Laurinen & Näsänen, 1982; Carrasco & Frieder, 1997) and changes in macaque cortical receptive field sizes (from Hubel & Wiesel, 1974b; see Scobey, 1982). The IMF for cortical magnification neither describes changes in cortical receptive field size (Dow, Snyder, Vautin & Bauer, 1981) nor changes in retinal ganglion cell density (Azzopardi and Cowey, 1993).

(3) Physiological Uncertainty. There is still considerable dispute concerning the magnification of the human cortex. This dispute partly persists because the IMF depends upon the precision of the foveal estimate

which is difficult to obtain physiologically.

(4) Interspecies Variability. Using functional magnetic resonance imaging, Sereno et al. (1995) estimated the MFs of several human visual cortical areas. They found that human V1 MF was markedly different from the macaque or the owl monkey MF. The macaque monkey MFs have been used successfully to describe human psychophysical data. Given the difference in MFs between monkeys and humans, it is quite surprising that estimates of monkey IMF succesfully explain certain human data.

(5) Individual Variability. Estimates of E_2 are based on the responses of a small number of participants and hence susceptible to individual differences. Most of the studies summarized in Table 1 used three or fewer participants and attributed a great deal of significance to small differences in E_2 between individuals. For example, Whitaker, Rovamo et al. (1992) compared one naive participant to one trained participant in two vernier acuity tasks. In the first task, they obtained E_2s of 1.23 for the naive participant versus 1.55 for the trained participant. In the second task, they obtained E_2s of 1.06 for the naive participant versus 1.96 for the trained participant[2]. Whitaker, Rovamo et al. (1992) concluded that practice effects were present. If E_2s vary between participants, by chance this order of results will occur 25% of the time. Therefore, generalizing from a small number of participants may not be justified. It would have been simple to test the same participant twice, once without practice and the other after considerable practice, and report a statistical test given the collected data. Grüsser (1995), using migraine phosphenes, found considerable foveal cortical representation differences between his three participants.

[2]The values for the other two trained participants were excluded because their E_2s were determined in a task where no positional jitter was added. This methodological change may increase the E_2.

(6) Similarity of IMFs. As mentioned earlier, the E_2 value derived in a particular task has been used to constrain the possible brain regions that limit performance in the task. It may be inappropriate, however, to attribute similar causes of eccentricity-dependence in performance to similar E_2s because several different mechanisms may share similar E_2s. For example, in cats area 17 and area 18 have identical IMFs (Mulligan & Sherk, 1993). The IMF in this case cannot be used to discriminate between area 17 and 18 in cats, although it can be used to rule out particular areas.

(7) Blending of IMFs. Because several MFs may limit performance in a given task, it is conceivable that their effects may average out and be well compensated for by an IMF that does not relate to a specific brain locus. Indeed, given all the factors influencing performance in a given task, it seems quite surprising that any psychophysically derived IMF may be directly associated with a single brain region (cf. Rovamo et al., 1978; Rovamo et al., 1997). This point is central to the investigation of complex perceptual phenomena, and is discussed more fully in the following section.

Blending of IMFs

Research Problem. A problem arises when multiple IMFs interact to determine performance changes with eccentricity in a given task. Can a single IMF accurately represent all of the sources of acuity loss associated with a single task? This point was raised before by several researchers (Westheimer, 1982; Mäkelä et al., 1993; Yu & Essock, 1996) but statistical methods for testing the ability or inability of a single IMF to compensate for performance changes with eccentricity are scarce in the litterature.

Consequence of Blending IMFs. Theoretically, two anatomically-based IMFs that interact in a psychophysical task will result in an intermediate IMF.

The relative influence of one versus another IMF on task performance will determine the nature of the intermediate IMF through a weighted average. For example, a task may depend on cone sampling and cortical sampling simultaneously. Stimuli constructed to have a greater dependence on cone sampling will reveal IMFs closer to the cone density's IMF, whereas stimuli constructed to have a greater dependence on cortical sampling will reveal IMFs closer to cortical sampling's IMF. Theoretically, a stimulus configuration exists that will reveal any intermediate IMF. This concept of blending IMFs, however, still remains to be supported by experiments.

For example, the fit of the detection of geometric distortions in faces (Rovamo et al., 1997) with the retinal ganglion cell density does not necessarily mean that geometric distortions are detected in retinal ganglion cells. Indeed, if performance was due to an interaction of the cortical magnification (in V1 or in higher cortical areas) and the cone density, interactions where the cortical influence is reduced would give rise to an intermediate IMF that easily could resemble the retinal ganglion cell density's IMF. However, to measure the limitations of the "geometric distortion" cells, all other sources of limitations have to be factored out.

Detecting Multiple Stages. One way to determine whether two or more stages interact in a given task is to change the nature of the interaction and see if the IMF is modified or not. It is known that retinal and cortical mechanisms mediate performance in different tasks, as shown in Table 1, but it is also possible that individual tasks may be influenced by both acuities at the same time. It is indeed surprising that a single magnification can account for distortions and undersampling, which can be due to several factors, including the blur of the image due to the optical properties of the eye's lenses, retinal cone or rod density, retinal ganglion density, LGN cell density

and cortex cell density, receptive field size as well as other factors.

A second way to determine if several stages influence a given task uses binocular integration. The human visual system is equipped with two eyes yet the percept of our environment is unitary. Information from the two eyes is integrated at a certain point in the processing of visual information. This integration can influence performance levels in psychophysical tasks and can create illusions of depth when disparate information is given to the two eyes.

Even though a single IMF might account for most eccentricity-dependent variability in a task, it cannot reveal all of the mechanisms that limit performance in that given task. The present thesis proposes a methodology that permits the recovery of several resolution limitations simultaneously. To demonstrate this, a task is presented where stimulus discrimination is limited by two factors. Then, a "multiple" methodology is presented that can recover these two limitations. Subsequently, an experiment is presented where several hypotheses pertaining to the two stages and the methodology are tested. Finally, the effects of binocular integration are explored as well.

Subjective Contours Defined by Offset Gratings

The perception of subjective contours (SC) produced by shifted gratings or by aligned line-endings has been extensively studied recently (Gurnsey, Humphrey and Kapitan, 1992; Gurnsey, Iordanova & Grinberg, submitted; Grosof, Shapley & Hawken, 1993; von der Heydt & Peterhans, 1989; von der Heydt et al., 1984; Wilson & Richards, 1992). SCs are formed when a discontinuity in a texture creates a percept of a contour, sometimes perceived as a luminance contour. However, unlike real luminance contours, SCs occur

in the absence of average luminance changes. SCs can easily be recovered computationally (von der Heydt & Peterhans, 1989; von der Heydt et al., 1984; Gurnsey et al., 1992; Gurnsey et al., submitted; Wilson & Richards, 1992). SCs of this kind have been shown to be detected in area V2, but not in area V1, in macaque monkeys (von der Heydt et al., 1984; but see Grosof et al., 1993).

The encoding of SCs has been modeled by several researchers (Francis & Grossberg, 1996; Gurnsey et al., 1992; von der Heydt et al., 1984; Wilson & Richards, 1992). Such models typically involve two stages of processing. Generally, the first stage involves linear orientation-selective filters identified with V1 simple cells. These respond well to the carrier (grating or lines) but poorly at the locus of the phase shift, as shown in Figure 4C and 4D. The output of the first stage is passed through a nonlinearity (squaring, halfwave-rectification or fullwave-rectification). The second stage uses linear orientation-selective filters to detect discontinuities in the first stage's responses that occur at the locus of the phase shift. The second stage is associated either with V2 contour cells (von der Heydt & Peterhans, 1989) or V1 complex cells (Grosof et al., 1993). The specifics of the modelled first and second layer filters are relatively unimportant for the purposes of the present research.

SC Model with Eccentricity-Dependence

SCs and Scaling. If in fact SCs are encoded in a two stage process and if the two stages are identified with different brain regions then these stages may scale differently with eccentricity; i.e., they may be characterized by different E_2 values. Resolution limitations of the first layer filters would be generally associated with receptive field size and wavelength selectivity of V1 simple cells. These limitations would be revealed in a grating acuity task.

When grating acuity has been studied across eccentricities, E_2s in the range of 2 to 5 have been found. Therefore, whenever the SC resolution is lost because of grating acuity limits, IMFs with E_2s between 2 and 5 should compensate for this loss. Little is known about how the mechanisms responsible for encoding SCs' change with eccentricity. There is some evidence that they are encoded either in V2 contour cells or V1 complex end-stopped cells, both of which are believed to take their inputs from V1 simple cells. Hence, SC cells may be limited either by V1 or by V2 cortical magnification. Because IMFs associated with cortical magnification in V1 and V2 are generally steeper (smaller E_2) than those associated with receptive field size, limitations arising from second-stage filters should show a steeper IMF.

Computational Model. Gurnsey, Iordanova and Grinberg (submitted) showed that SCs detection performance dropped in two cases: (1) when the carrier wavelength was too short and (2) when the SC length (or aperture size) was too small. Also, in agreement with past research, they found that once 7 to 15 line terminators form the SC, adding more line terminators (i.e. increasing SC length)[3] doesn't increase performance (von der Heydt & Peterhans, 1989; Gurnsey et al., submitted; Soriano et al., 1996). In other words, they concluded that performance reaches an asymptotic level once a threshold number of terminators are present.

To investigate the effects of grating acuity and contour length on SC discrimination, a generic model of SC detection is presented. The model to be examined is essentially that of Wilson and Richards's (1992) with minor modifications. The first stage consists of two filters having phase preferences which are shifted by 90° with respect to each other (Figure 4B). Such filters are

[3]SC length can be defined in terms of line terminators or degrees of visual angle. Line terminators describes the stimulus in terms of object features assuming some scale constancy. The other assumes cells encoding SCs that prefer a certain contour length which is independent of the carrier wavelength.

said to be a "quadrature pair" because they are a quarter of a cycle out of phase. The receptive field of V1 simple cells can be approximated by Gabor signals[4] (Marcelja, 1980) and are reported to be arranged in quadrature pairs (Pollen & Ronner, 1981; 1982; 1983; Burr, Morrone & Spinelli, 1989) at all eccentricities (Morrone, Burr & Spinelli, 1989; but see Bennett & Banks, 1987). When the receptive field of a cell is known (Figure 4B), its response to any stimulus can be determined. When this is done over the whole image, termed convolution[5] (Figure 4C), local Fourier "energy"[6] can be computed by adding the squared responses from the two filters (Figure 4D). This strategy provides a phase-independent measure of a spatial frequency energy at each image location (Figure 4D). As noted by Wilson and Richards (1992), energy drops at the SC location. This drop in response is encoded by the second stage filter (Figure 4E) having the same form as the first layer filters but differing in orientation selectivity and scale. As a result of these computations, the properties of the SC are made explicit (Figure 4F).

---

[4]A Gabor is a Gaussian-modulated sine-wave grating whose's amplitude is given by: $G(x, y) = \cos\{[2\pi x / \omega] + \alpha\} * \exp\{-[x^2 + y^2] / [2\sigma^2]\}$, where σ is the window size, ω is the wavelength and α is the phase of the filter. When $\alpha = 0°$, called "Even Gabor", equidistant points from the middle of the Gabor have the same polarity. When $\alpha = 90°$, called "Odd Gabor", equidistant points from the middle of the Gabor have reversed polarity. Even Gabors prefer line stimuli, while Odd Gabors prefer edge stimuli.

[5]Cells respond best when stimulus luminance profiles match the excitory and inhibitory regions of the cell's receptive field. A convolution computationally mimicks this function and gives a measure comparable to firing rate at each point of the image. The convolution is given by: $F(x, y) * G(x, y) = \iint_{-\infty}^{\infty} F(\alpha, \beta)\, G(x-\alpha, y-\beta)\, \delta\alpha\, \delta\beta$.

[6]Fourier energy is the amplitude of the sine-wave component in the image that matches the specified orientation and wavelength. This measure is independent of phase.

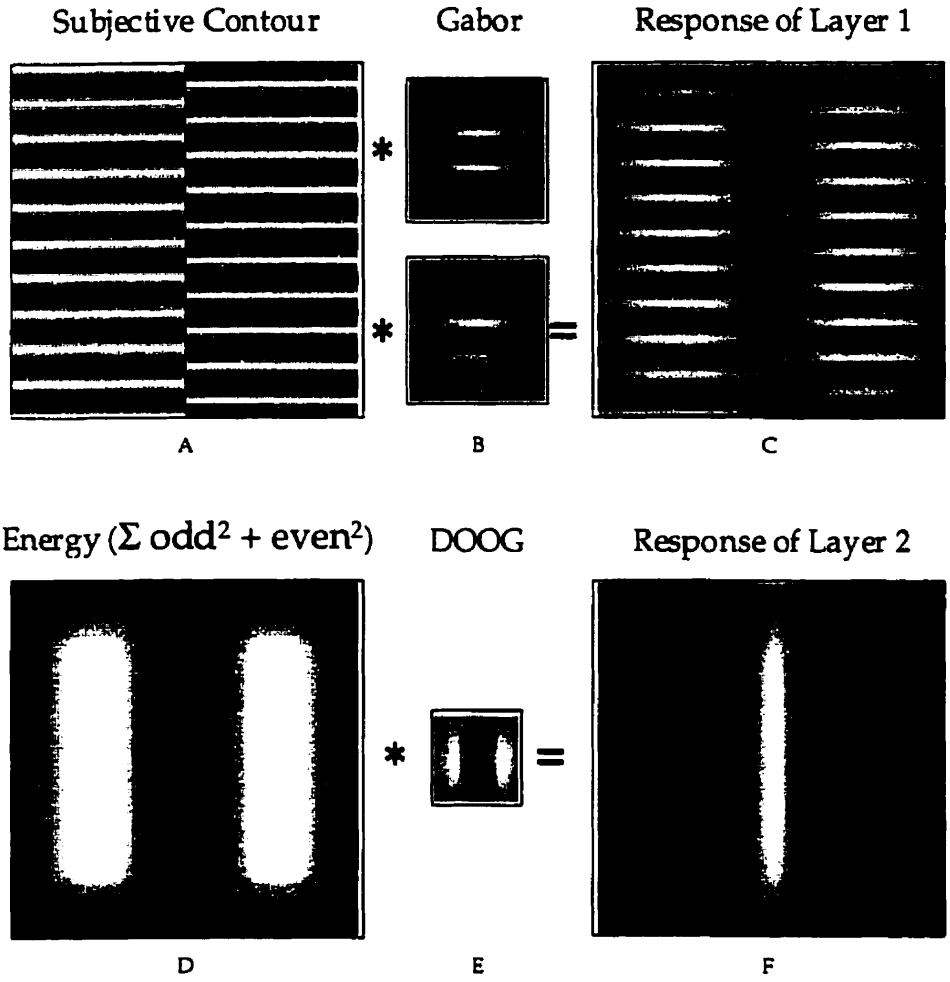

Figure 4. A model of SC encoding. SCs (A) are thought to be extracted via multiple layers of spatial filtering. An orientation selective Gabor filter (B) is applied to the image and the response of the Even component is shown in (C). When local energy is computed [Energy = ($Even^2$ + Odd^2)] a trough in the energy response is seen at the locus of the SC (D). When this energy response is convolved with a second layer filter tuned to vertical (E), a positive response to the SC is seen (F).

Wavelength and SC Length. For a given SC length, the model presented in Figure 4 would respond best when the wavelength sensitivity of the first layer filters matches the wavelength of the carrier grating in the stimulus. Moreover, for a given carrier, the response of the mechanism will be maximal when the length of the SC covers the second layer filter's receptive field. Therefore, reducing the wavelength, SC length or both below a certain point will reduce the response of the mechanism. To demonstrate

this, grating wavelength and SC length were systematically varied (Figure 5A-D) and the response of the mechanism was recorded. This parallels the type of psychophysical experiment described below in which SC discrimination thresholds are measured for a range of contour lengths and carrier wavelength at different eccentricities.

Detection or discrimination thresholds are assumed to correspond to a fixed response strength from the model. The dark lines overlaying the plots in Figure 5 depict iso-response lines. Assuming that this level of response represents threshold, the line depicts all combinations of wavelength and size producing threshold responses. When SC length is increased, the threshold wavelength decreases and asymptotes to a value greater than 0 (i.e. wavelength must be greater than a positive value). Conversely, when wavelength is increased, the threshold SC length decreases and asymptotes to a value greater than 0 (i.e. SC length must be greater than a positive value). The same form of curve has been found in many psychophysical experiments in which two limits simultaneously govern performance. For example, in a task where participants had to discriminate between right- and left-oblique lines, both line length and orientation difference could limit performance and both values asymptoted when the other was optimal (Mäkelä et al., 1993). Moreover, the asymptotic values for line length and an orientation-difference were both larger than 0. Also, a smooth transition occurs between the limit of SC length and the limit of wavelength[7].

SCs and Eccentricity. The limits are proposed to change with eccentricity of presentation. As mentioned above, the size of the two mechanisms may scale differently with eccentricity (i.e. have different IMFs)

[7]This form of curve can be obtained by multiplying two probability functions (s-shaped like a logistic function or a Weibull function) and fixing a threshold value above base rate. The same smooth transition and limits are observed.

because they are assumed to represent physiological limitations imposed by two different visual areas. To examine the consequences of this situation, the first and second layer characteristics were scaled according to different E_2s and the preceding analysis was repeated for a number of simulated eccentricities. The first layer was scaled with an E_2 of 2.5 and the second layer was scaled with an E_2 of 0.5. Table 2 presents simulations of the response surface for the SC encoding model presented above. The columns present in order the simulation number (entry), the wavelength of the first layer filters, the length of the second layer filter, the ratio of second layer length to first layer wavelength, the simulated eccentricity (if applicable) and the intercorrelations between response surfaces when scaled (see below). The simulation entries 4 to 7 represent eccentricities of 0° to 6°. The other characteristics of the filters were proportional to their wavelengths or lengths. The maximum response, the stimulus size and the wavelength at which performance declined all changed with eccentricity. When expressed in logarithmic coordinates, the threshold size increased at a faster rate than the threshold wavelength.

If a similar experiment were to be performed by participants, their threshold curves should vary in a similar way if in fact a model of the sort described determines performance *and* the first and second layer filters scale at different rates. It is important to note that the change in the response surface of the model is well-predicted by the use of scaling. If the "wavelength" axis is scaled using the same E_2 used to scale the first layer filter and the "SC length" axis is scaled using the same E_2 used to scale the second layer filter, then the response surfaces become perfectly correlated (see Table 2: all R^2_{adj} were above 93.4%). Conversely, the performance curves can be used to estimate the IMFs for the "wavelength" and "SC length" axes through extracting the limits at each eccentricity. More concretely, if our visual system

requires a larger SC length increase with eccentricity than wavelength increase, the response curve will shift faster along the SC length axis than along the wavelength axis (in log coordinates).

Table 2: Values Used in Simulations

	1st Layer	2nd Layer	Ratio	Ecc.	R^2 adj (%)					
Entry	Wavelength	SC Length	2nd / 1st		1	2	3	4	5	6
1	10	20	2.00							
2	10	12	1.20		98.97					
3	15	6	0.40		96.90	97.24				
4	10	6	0.60	0°	96.66	97.09	93.49			
5	12	12	1.00	2°	96.77	96.70	93.87	98.56		
6	14	18	1.29	4°	97.38	96.93	94.49	98.29	99.09	
7	16	24	1.50	6°	97.32	96.99	94.44	98.13	99.02	99.19

Note: The wavelength of the grating varied from half that of the Gabor filter to the same wavelength as the Gabor, in 20 steps. The values of the size of the grating changed from 0 to twice the size of the DOOG in 10 steps.

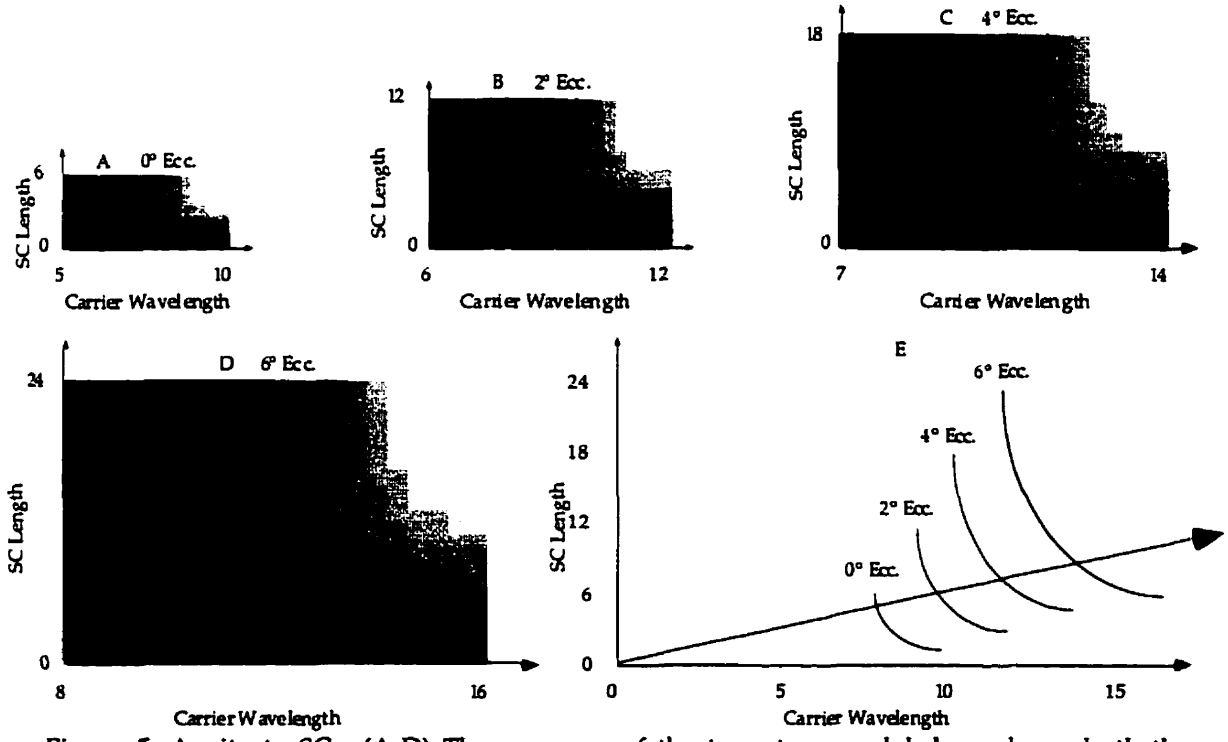

Figure 5. Acuity to SCs. (A-D) The response of the two stage model depends on both the

wavelength of the carrier and the length of the SC. Responses are shown for wavelength from half to the full wavelength of the first layer filters, and from 0 to the length of the second layer filter. Shown in panels from A to D are simulations for eccentricities of 0° to 6° of eccentricity (in steps of 2°) assuming an E_2 of 2.5° and of 0.5° for the first and second layer filters respectively. (E) The curves are represented on the same graph for comparison. Over the range of eccentricities considered, it is clear that the response curves shift at different rates along the two axes, otherwise the arrow would intersect the same part of the curve. However, scaling reveals that the same IMFs used to describe the changes of scale of the two mechanisms can be used to account for the shifts in the performance surfaces (see Figure 7 for details on scaling data limited by two IMFs).

Simultaneous Recovery of Two Acuity Limits

(1) Rectangular Parabola. Research on eccentricity-dependent changes in performance often measure acuity limits. For example, in grating acuity tasks the minimum resolvable wavelength is measured (see Table 1), which is typically thought to reflect retinal ganglion cell spacing or the high frequency cutoff of spatial frequency simple cells in the cortex. This represents one limiting dimension. When SCs are encoded, both wavelength-selective cells and SC cells can limit performance, i.e. second layer filters will give a poor response if the carrier wavelength is too short[8] or the SC length is too short. In such cases where more than one limiting dimension exists, the rectangular parabola (Serway, 1992) can be used to recover the limits separately. This is similar to measuring the asymptotic values in Figures 5 and 6. The rectangular parabola has the form:

$$(s - s_{min})(\omega - \omega_{min}) = \xi^2, \qquad \text{[Eq 3]}$$

when 2 dimensions are considered. ω and s are the stimulus wavelength and SC length at threshold respectively, ω_{min} is the minimum wavelength

[8]Increasing wavelength beyond the wavelength of the first-layer filters will reveal a U-shaped curve at fixed levels of performance. However, other mechanisms with larger wavelength-preference would be expected to respond within that range, making the function near-asymptotic over a range of wavelengths. Because only the limits in the short wavelengths are considered, the asymptotic approximation holds and the rectangular parabola can be used.

required for performance at threshold and s_{min} is the minimum SC length required for performance at threshold. ξ^2 is a constant relating ω and s at intermediate values (see Figure 6A). When the rectangular parabola is plotted in log-log space (see Figure 6B), it is roughly linear (slope ≈ -1) within a range of values (near $\omega - \omega_{min} = s - s_{min}$), becomes non-linear closer to the minimum values ($s \approx s_{min}$ or $\omega \approx \omega_{min}$) until it asymptotes with a slope of 0 or $-\infty$. This function has the advantage that it is symmetrical about the oblique (45°) axis passing through its middle, and it is computationally simple to use[9].

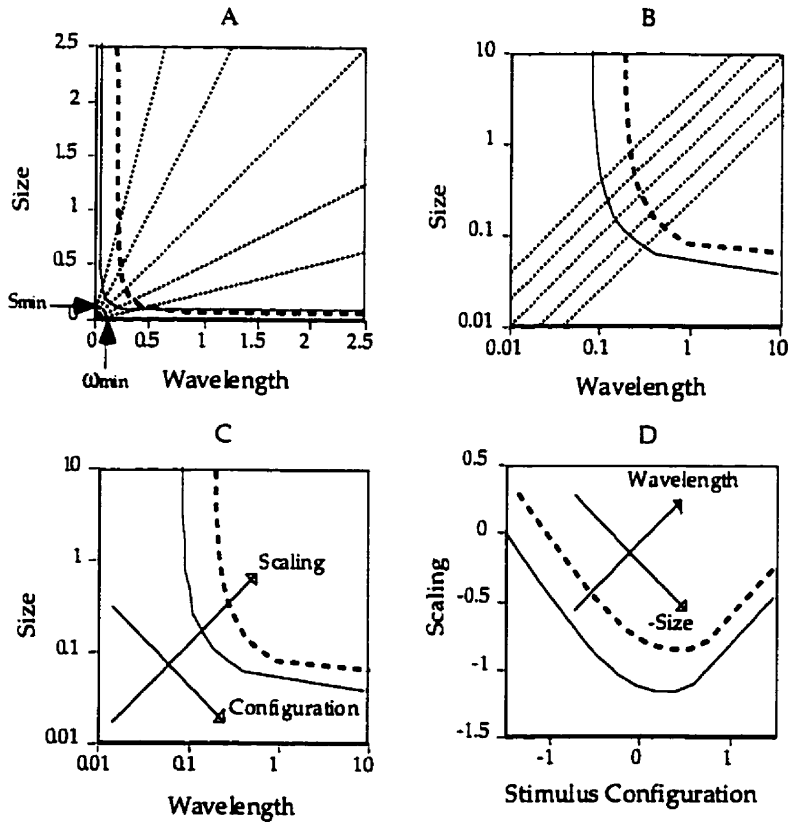

Figure 6. Rectangular parabola. (A) The solid line represents a line of constant response, as a

[9]In comparison, the function used by Mäkelä et al. (1993) was asymmetrical and the function used by Paradiso (1988) was computationally complex. Mäkelä et al.'s (1993) formula uses a function similar to the rectangular parabola except that one of the differences between stimulus and its limit is squared. This makes the function asymmetrical along its middle. For this reason, if axes would be interchanged, the solution would be different. Paradiso (1988)'s fit was made through a complex model of orientation which included variables such as variability of single cell responses and number of cells over whose responses was integrated. That type of model contains too many variables for the present purposes and cannot easily be reduced to as simple a formula as the rectangular parabola.

function of SC length and carrier wavelength, from the model shown in Figure 5. This level of responding may also be taken to represent threshold performance in a psychophysical task. The limits (s_{min} and ω_{min}) are shown. Another rectangular parabola with larger s_{min} and ω_{min} is shown (thick dotted line). Rectangular parabolas are shown in linear coordinates. The function clearly asymptotes along the wavelength and size axis, i.e. SCs cannot be recovered when either the size or the wavelength is below a certain limit (thick lines). The sampling lines (thin dotted lines) represent the space shared by stimuli containing the same number of cycles within their aperture but differing in scale. (B) When expressed in log-log coordinates, the sampling lines chosen are parallel to each other and equidistant. They are also approximately perpendicular to the rectangular parabolas. (C) For analytical purposes, the data are expressed in a new coordinate system: the stimulus configuration and the scale of the stimulus (see text for more details). (D) When data are re-expressed in terms of stimulus configuration and scale, the configuration-shift in the curve becomes more apparent, shown by the horizontal shift of the curve's minimum.

(2) Prediction and Error from Prediction. The rectangular parabola depicted in Figure 6A-C presents two problems when one attempts to employ it in psychophysical experiments in which detection or discrimination thresholds are limited by two stimulus dimensions; for example, SC length and carrier wavelength. Such data could be collected by determining threshold contour size for each carrier wavelength, or, conversely, threshold carrier wavelength for fixed contour lengths. Regardless of which strategy is adopted threshold will be difficult to determine as one approaches the asymptotic value of the fixed dimension. For example, as ω_{min} is approached it will be very difficult to establish threshold size because of the steepness of the curve (expressed as a function of ω) at that point.

An alternative sampling strategy can be employed to deal with this problem. The linear dotted lines in Figure 6A-B depict stimuli in which the relationship between the two variables is fixed and only the scale (size) of the stimuli differ. In the example of SCs differing in size and carrier wavelength, each of the dotted lines represents stimuli with a fixed number of cycles of the carrier within the stimulus aperture. The stimuli increase in size as one moves away from the origin of this space along the line. One advantage of

this sampling strategy is that each sampling line intersects the rectangular parabola which describes the performance limits. Therefore, if the stimulus space is sampled in this way a threshold will be found along each sampling line, in contrast to a strategy that samples parallel to one axis or the other. Note that in Figure 6B that when the axes of the stimulus space are expressed on logarithmic scales the sampling lines become parallel and--if the angles of the sampling lines are appropriately chosen--equally spaced. Once data have been collected in this way, however, the problem of how to determine the parameters of the best fitting rectangular parabola arises.

One possiblitiy would be a conventional least squares approach in which one selects the rectangular parabola that minimizes the squared deviations of the sampled data point along lines that are perpendicular to the x axis. However, because the data have been collected with error along the x axis the rectangular parabola that in theory produced the data points may not be recoverable. For example, if a sampled ω value at threshold is found to be .1 at threshold, and the function that actually generated the sample point has ω_{min} = .2 the squared deviation of the sampled point from the generating function is undefined. Therefore, a different curve fitting procedure is required.

A reasonable strategy that overcomes this problem is to find the rectangular parabola that minimizes the sum of squared deviations of data points along each of the sampling lines. This strategy can be simplified (conceptually) by considering the projection of the log-log stimulus space onto an axis oriented 45° to the original space as shown in Figure 6C. In this rotated representation:

$$X = -\alpha \log (s/\omega) \text{ and} \qquad \text{[Eq 4]}$$

$$Y = \alpha \log (s\omega), \qquad \text{[Eq 5]}$$

where $\alpha = 2^{-0.5}$. X represents a particular sampling line or stimulus configuration (i.e., one of the dotted lines in Figure 6B). Y represents the scaling of this stimulus (i.e., position along one of the dotted lines in Figure 6B). In much of what follows SC stimuli will be discussed in terms of X and Y which will be referred to as *stimulus configuration* and *scaling* respectively. Figure 6D shows the rectangular parabola in (X,Y) space; i.e., configuration by scale.

When the stimuli are considered in (configuration, scaling) space or (X,Y) space (Figure 6D) it is easy to see how a least squares procedure could be employed to determine the best fitting rectangular parabola. A rectangular parabola (having parameters s_{min}, ω_{min} and ξ, see Equation 3) is represented in (X=configuration,Y=scaling) space as

$$Y' = 2\alpha \log \{s_{min} + \omega_{min}\mu + [(s_{min} + \omega_{min}\mu)^2 + 4\mu(\xi^2 - s_{min}\omega_{min})]^{0.5}\} - 2\alpha \log(2) - \alpha \log \mu, \text{ and} \qquad \text{[Eq 6]}$$

$$X' = -\alpha \log \mu, \qquad \text{[Eq 7]}$$

where $\mu = s/\omega$. For a given *scaling-threshold* (Y_{Thresh}) obtained along a particular sampling line (X), its deviation from the scale predicted (Y') by a given rectangular parabola (defined by s_{min}, ω_{min} and ξ) can be determined. For a set of thresholds collected along a number of different sampling lines, the rectangular parabola that minimizes the sum of their squared deviations can be taken as the one that provides the best fit to the obtained data.

This best fitting rectangular parabola in (X,Y) or (configuration, scale) space can be rotated back into the linear size (s) and wavelength (ω) space

using Equations 8 and 9:

$$\omega' = 10^{\alpha(X'+Y')}, \text{ and} \qquad [Eq\,8]$$

$$s' = 10^{\alpha(Y'-X')}. \qquad [Eq\,9]$$

(3) "Classic" vs "Multiple" Magnification. It is possible that only one stage of processing determines the magnification function that characterizes a task, as has often been assumed. This point of view will henceforth be referred to as the "classic" method. As reviewed earlier, however, several factors may limit performance in a psychophysical task. For example, vernier tasks may be limited by the sampling density of the cones and subsequently by cortical magnification. The "multiple" method presented here is able to detect the existence of several eccentricity-dependent limitations on performance. It also provides a basis for determining the IMFs required to equate performance across the visual field. In the SC task discussed below, the changes in ω_{min} and s_{min} with eccentricity are taken as characterizing the changes in properties of first and second stage mechanisms. A steeper IMF for one stage versus another can be taken as evidence that the two stages are separate. Conversely, if both IMFs are the same then only one eccentricity-dependent limitation exists for the task and the variables tested.

To demonstrate the appropriateness of the data fitting procedures defined in the preceding section, several parabolas representing different eccentricities were generated using the parameters $\omega_{min} = 1$, $s_{min} = 2$, $\xi = 1$, $E_{2\omega} = 2.5$ and $E_{2sc} = 0.5$. Figure 7A shows simulated data for eccentricities of 0°, 2.5°, 5°, 10° and 20°. A least-squares method can be used to determine the values of ω, s, ξ, $E_{2\omega}$ and E_{2sc} that best fit the simulated data. The classic method is equivalent to assuming that both axes scale the same way (i.e. $E_{2\omega}$ =

E_{2sc}), while the multiple method does not impose this constraint (i.e. $E_{2\omega}$ may or may not equal E_{2sc}). Figure 7B shows the data transformed into (X, Y) coordinates (as described in Equations 4 and 5). Finally, using the IMFs, these data points are collapsed onto the foveal condition to show the goodness of fit for the classic (Figure 7C) and the multiple method (Figure 7D).

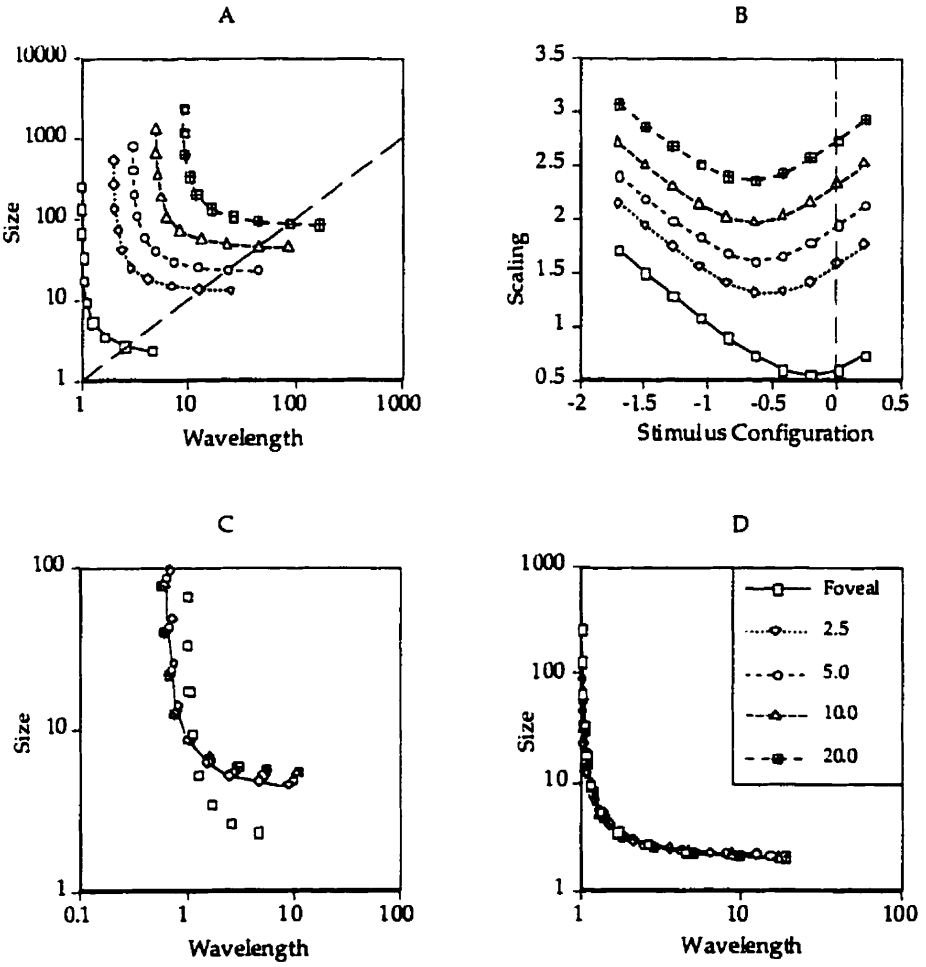

Figure 7. Model of rectangular parabola and two IMFs. (A) Unscaled simulated data. (B) Data are rotated to show the curve shift along the configuration axis. (C) "Classic" method: the same scaling is applied on both axes. Ideally, the data points should follow the line to show that all eccentricity-dependent variability was accounted for. (D) "Multiple" method: different scalings were applied to the two axes, which was enough to eliminate the eccentricity-dependent variability.

Figure 7C shows that the classic method can greatly reduce the eccentricity-dependent variance, even when two independent E_2s are present.

It is clear, however, that the classic method produces a less than perfect fit to the data. The classic method derives an E_2 of 0.937° which is intermediate between the two actual E_2s (2.5° and 0.5°) and inaccurately estimates the characteristics of the foveal parabola. Therefore, even when the data are noise-free, the "classic" method is inaccurate in cases when several E_2s determine task performance.

Figure 7D shows that the data fitting procedure recovers a solution that eliminates all eccentricity-dependent variability in the data when it is set up to recover 2 E_2s. Furthermore, all parameters (ω_{min}, s_{min}, ξ, $E_{2\omega}$ and E_{2sc}) were recovered perfectly. Removing eccentricity-dependent variability in Figure 7A provides a general curve, as shown in Figure 7D. Similarly, apparently different response surfaces derived with the model and shown in Figure 5 collapsed into a single response surface when eccentricity-dependent variability was removed by the use of scaling.

(4) Appropriate and Powerful Testing Techniques. Experiments conducted on peripheral vs. foveal viewing often lack appropriate and powerful statistical testing to assess how well a function reduced eccentricity-dependent performance changes. Usually, researchers are content to report that their functions account for a significant amount of the variance and succesfully make functions overlap (as often judged by eye). A conventional measure of accounted variance (e.g. R^2) could be reported, but it would not differentiate between the sources of variance that are due to eccentricity or to curve shape. Moreover, claims such as: "eccentricity-dependent variability was removed" are rarely accompanied with statistical tests. Also, as explained above, it is possible that eccentricity-dependent changes may be in the form of interactions as well as main effects. Specifically, only a statistical test sensitive

to the change of the function's shape with eccentricity would detect cases where more than one IMF is required. However, such a test has not been designed previously.

A powerful technique would use all of the degrees of freedom from the data collected. This can be achieved by using eccentricity and stimulus configuration (X; see Equation 4) as independent variables, and scale (Y; see Equation 5) as a dependent variable. These variables can be analyzed in an ANOVA. Main effects describe the effects of eccentricity and the effects of stimulus configuration independently. The interaction between eccentricity and stimulus configuration describes systematic curve shape changes with eccentricity. The presence of an interaction provides unambiguous evidence that one IMF is insufficient to describe changes in mechanisms with eccentricity[10]. Indeed, as seen above, the curve shifts along the configuration axis when two IMFs are used to generate the data, a change readily detectable with the measure of interaction. Also, if a line is fitted to data at each eccentricity, the slope will monotonically change as a function of eccentricity if two E_2s are present and if sampling is relatively near the point where the slope of the rectangular parabola is -1 in the log-log space. Based on this fact, the "change of slope" test was designed to detect the presence of several IMFs in the task. Finally, an ANOVA on the residuals will show if the model used to fit the data accounts well for systematic variability. A parallel analysis using curve fitting can reveal the values of E_2s and of the foveal rectangular parabola.

(5) Least Squares Method. To recover the parameters as described in Figure 7, a data fitting procedure was used. The same analysis can be applied

[10]However, the presence of an interaction is not sufficient to conclude that two or more IMFs are required to explain performance changes with eccentricity. For example, an interaction would appear if the curve would change from highly curved in the fovea to linear in the periphery. A more specific test is designed ("slope change test") and data fitting techniques are applied to deal with this issue.

to psychophysical thresholds. The purpose of this analysis is to quantify the way in which SC length and carrier wavelength must be scaled with eccentricity to maintain threshold level performance.

To review, Equation 3 ($(s - s_{min})(\omega - \omega_{min}) = \xi^2$) defines a rectangular parabola. The rectangular parabola is assumed to capture the general shape of the curves defining the locus of "scaling" thresholds in the size (s) by wavelength (ω) SC space.

Equation 10 (slightly altered reproduction of Equation 2) shows how E_2 can be used to equate stimulus discriminability across the visual field. E_2 has been used to determine how stimuli must be scaled with eccentricity to maintain performance equivalent to that measured at the fovea.

$$\phi_e = 1 + e / E_2, \qquad \text{[Eq 10]}$$

Equations 3 and 10 together provide a basis for describing the scaling thresholds along each of the sampling lines and at each eccentricity as found in the experiment. The classic method implies that a single IMF (described by Equation 10) is sufficient to equate SC discrimination across eccentricities. Therefore, if s_{min}, ω_{min}, ξ and E_2 happened to be known then Equation 11 provides a description of threshold size and wavelength combinations at each eccentricity (e).

$$(s - \phi_e s_{min})(\omega - \phi_e \omega_{min}) = \phi_e^2 \xi^2, \qquad \text{[Eq 11]}$$

The multiple method described in the introduction (see Figure 7) provides for the possibility that each dimension of the stimulus that limits performance might be characterized by a different E_2. In the present case the size and wavelength dimensions might be characterized by different E_2

values. These are represented in equations 12 and 13. The only difference between these two equations and Equation 10 is that subscripts have been added to associate scaling factors (ϕ_e) and E_2s, with specific dimensions.

$$\phi_{s\,e} = 1 + e / E_{2s}, \qquad \text{[Eq 12]}$$

$$\phi_{\omega\,e} = 1 + e / E_{2\omega}, \qquad \text{[Eq 13]}$$

Given that performance may depend on two scaling factors, Equation 11 can be rewritten as Equation 14 to reflect this fact.

$$(s - \phi_{s\,e}\, s_{min})\,(\omega - \phi_{\omega\,e}\omega_{min}) = \phi_{s\,e}\,\phi_{\omega\,e}\,\xi^2, \qquad \text{[Eq 14]}$$

Equation 14 provides a *model* of the loci of size and wavelength threshold pairs at each eccentricity (e). The model described in Equation 14 can be used to fit the data collected in the Experiment. That is, a search procedure can be used to find the parameters s_{min}, ω_{min}, ξ^2, E_{2s} and $E_{2\omega}$ that minimize the error between data and model. The only question to be answered in this context is: "What measure of error should be taken?" The obvious answer is to minimize the sum of squared deviations of individual data points from model predictions (i.e., Equation 14) *along the sampling lines* (as determined in the section "Prediction and Error from Prediction" above). In other words, within the model, the predicted threshold along a particular sampling line for a given eccentricity is determined by the parameters s_{min}, ω_{min}, ξ^2, E_{2s} and $E_{2\omega}$. Thefore, the data fitting procedure must find values for s_{min}, ω_{min}, ξ^2, E_{2s} and $E_{2\omega}$ that minimize the sum of the squared deviations of individual data points from their position predicted by the model along the sampling line.

The foregoing development described model fitting in size and wavelegth space. In fact, fitting was actually done in configuration (X) and

scale (Y) space (see Equations 6 and 7) and the results transformed back into size and wavelength space (Equation 8 and 9). This implementation detail makes no difference to the resulting solution. Search for the best-fitting parameters was carried out using the "Solver Plugin" of Microsoft Excel version 5.0[11].

Experiment

The goals of this experiment are threefold. (1) To introduce a methodology to assess the changes on two or more dimensions that may simultaneously limit performance in a task. (2) To assess the effects of eccentricity on the SC formation. (3) To challenge the widespread belief that performance in a task is well-explained by one IMF.

Method

Participants. 5 participants volunteered (mean age = 28.6, st.dev. = 9.3). Their vision was normal or corrected to normal as judged by their optometrist, and participants who needed corrective glasses or lenses wore them throughout the testing sessions.

Apparatus. Testing and data collection was done using an Apple PowerMacIntosh 7100/80 equipped with a 1024 x 768 pixel color monitor (27 pixels/cm, refresh rate = 75 Hz).

Stimuli. SCs defined by offset gratings were used. Two perpendicular sinusoidal gratings of identical wavelength, one vertical and the other horizontal, were added within a circular aperture. Sinusoidal gratings were used to reduce aliasing due to subsequent manipulations done on the stimuli and to reduce the effects of other spatial frequency components (i.e. to reduce the spread in the frequency domain) to ensure that only a limited group of wavelength-selective cells encoded the stimulus. As shown in Figure 8, from

[11]The Solver Plugin is susceptible to local minimums. For this reason, the fitting was repeated until it was determined that the best solution was achieved.

one side to the other of the diagonal diameter (±45°), the phase of the gratings was shifted by 180° (equivalent to a change of polarity). SCs could be right- or left-oblique. The fixation point was a 2x2 pixels white square within a 4x4 black square and was placed in the same depth plane to control for accomodation. Average screen luminance was 31.5 cd/m^2.

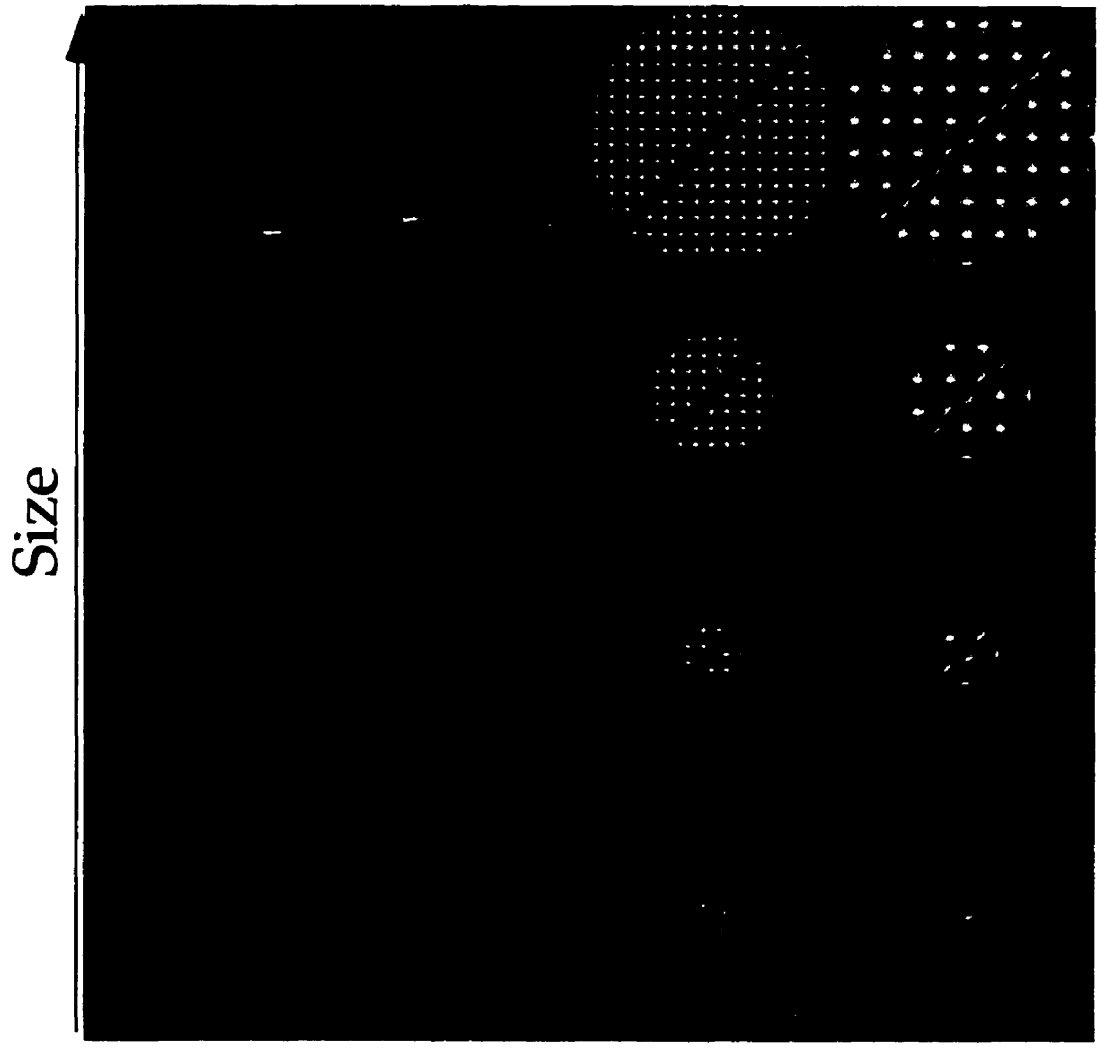

Figure 8. Stimulus space (in log-log coordinates). Several axes can be used to describe the stimuli: (1) size refers to the aperture size or the SC length, (2) wavelength refers to the carrier wavelength, (3) scaling refers to the sampling strategy used in the experiment, namely, a scale change without change in configuration of the stimulus, and (4) stimulus configuration (perpendicular to the scaling axis) which refers to the number of cycles within the aperture (cpa).

Procedure. When the fixation point was foveated, participants pressed a key to initiate a trial. The fixation display was replaced by the stimulus display for 13.3ms, immediately after which the fixation display reappeared. No mask was used. After a short time a second stimulus appeared for the same duration[12]. Participants had to decide which of the two displays presented on a trial contained the right oblique SC, the other containing a left oblique SC (forced-choice). Sampling lines (stimulus configuration) corresponds to ω/s of .25, .5, 1, 2, 4, 8, 16 and 32 expressed in cycles per aperture (cpa). A modified BEST PEST[13] adaptive threshold procedure (Lieberman & Pentland, 1982) was used to find the threshold scale on each sampling line. A Weibull function was used as the underlying psychometric function and the 81% part of the curve was taken as threshold.

The five eccentricities tested were foveal (0°), 2.5°, 5°, 10°, and 20° in the nasal visual field (temporal retina). At each eccentricity the 8 sampling lines were interleaved.

To reduce the range of stimulus required to calculate the IMF, viewing distances were set using:

$$D(e) = Df / (1 + E / E_2), \qquad \text{[Eq 15]}$$

where E_2 is set to 2.5 and Df is 100cm. These values were chosen based on

[12]13.3ms is too short a time to allow for unintentional saccadic eye movements (see Carrasco & Frieder, 1997 for references) but creates an afterimage which remains on the retina for inspection.

[13]The BEST PEST was found to be more efficient than a standard staircase procedure, the original PEST and an improved PEST (Pentland, 1980) in a simulation. It was also found to be as accurate as the QUEST (Watson & Pelli, 1983) procedure and could adjust to gradual improvements in performance (Madigan & Williams, 1987). However, after testing participants with a step method which assumes an unrealistic psychometric function and finding that several psychophysical methods converged equally well, as measured by the accuracy and the number of trials, Simpson (1989) concludes: "it is heartening that one need not be overly concerned about which psychophysical method one chooses" (p.576).

pretesting. A binocular foveal condition was added to explore the effects of binocular integration on the percept of SCs.

The SC length ranged from 0° to 19.3°, and the longest wavelength possible was 5.9° for the individual gratings. A cycle of the composite grating is defined as the separation between two adjacent peaks, which equals sqrt(2) times the length of the underlying grating wavelength. Conditions were constructed either by changing the wavelength or the aperture size by steps of 2, giving ratios ranging from .25 to 32 cpa (≈.3535 to 45.25 cpa for the individual gratings).

Results

Presence of Two IMFs

An "Edgy" Situation. Figure 9A summarizes the results of the experiment. The average results for the 5 participants (±SEM) are plotted as a function of configuration (X) and eccentricity (foveal binocular condition also included). In Figure 9A it is evident that data do not follow the form of a rectangular parabola rotated in the configuration and scaling space. Figure 9B (also shown in Figure 11C) shows the same data in the SC length and wavelength space after they were collapsed into a single function. IMFs were measured using two E_2s and with outliers removed (see "Least-Squares Method" and "Least-Squares Results" below). For comparison, the data for the .25 and .5 cpa conditions were scaled using the IMFs derived from the least-squares fitting procedure (see "Least-Squares Method" and "Least-Squares Results" below) and shown in Figure 9B. After scaling, data from conditions of .25 and .5 cpa form a clear break with the rectangular parabola. Inspection of the lower two stimuli in Figure 9C reveals the cause of the break in the data

set: stimuli with less than 1 cycle per aperture (cpa) resemble luminance edges more than SCs. Therefore, such stimuli may be encoded by mechanisms such as V1 simple cells, which respond readily to a luminance edge. For this reason, separate analyses were performed on the negative configuration values, which will hereforth be referred to as "luminance edge stimuli", and the remaining 6 levels configuration, which will still be referred as SCs. The "reduced set" refers to the 6 levels of SC configuration. Subsequent analyses were performed on the reduced set. The binocular condition was also analyzed separately.

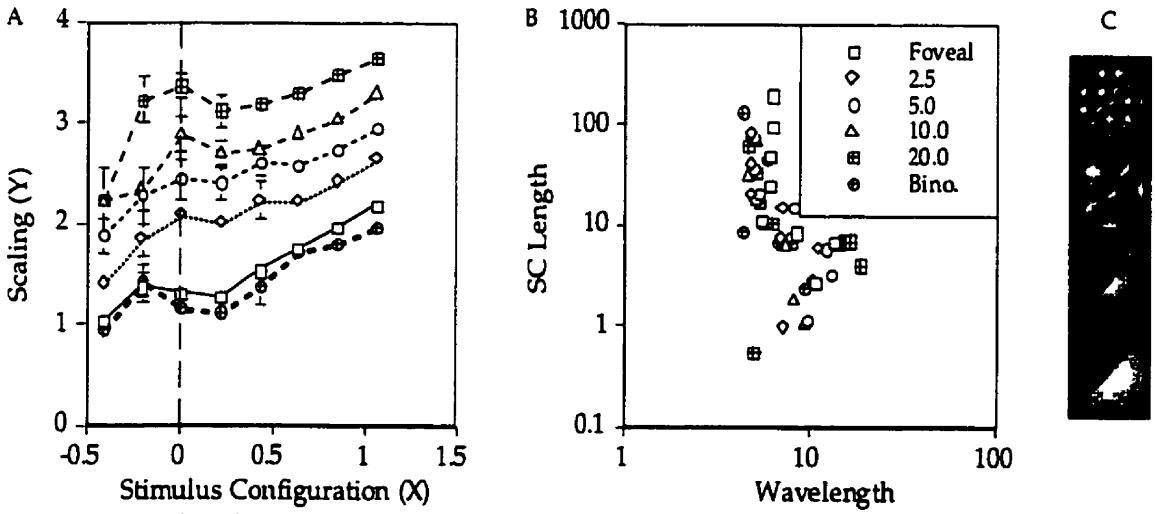

Figure 9. Results of Experiment 1. (A) Data set expressed in terms of stimulus configuration (X; sampling line; see Equation 4) and scaling (Y; see Equation 5) for eccentricities of 0°, 2.5°, 5°, 10°, 20° and for a binocular foveal condition. (B) The same data after independently scaling the two axes ("multiple" method; see text for more details), which makes the data sets for each eccentricity overlap. When this is done, a single function emerges (C) Stimuli are shown with fewer and fewer cycles per aperture size from top to bottom. The two lower stimuli are in the negative configuration range. Stimuli with negative configuration (X values) were discontinuous with the data line, as shown in (A) on the left of the dotted line and in (B) under the rectangular parabola-shaped data. This is readily understood, because these stimuli appeared very much like luminance edges.

Table 3: Eccentricity by Configuration ANOVA on Reduced Set

Source	*df*	SS	MS	F	p	ê
Subjects	4	1.075	.269			
Eccentricity	4	49.697	12.424	72.467	.0000	
Error	16	2.743	.171			.51
Configuration	5	7.037	1.407	40.823	.0000	
Error	20	.690	.034			.26
Interaction	20	1.002	.050	2.063	.0124	
Error	80	1.944	.024			.1

Eccentricity and Stimulus Configuration. Table 3 presents the results for the 6 (configuration or sampling line) x 5 (eccentricity) within-subject ANOVA[14] performed on the scaling (Y) data of 5 participants. Calculated using Equation 5, the dependent variable "scaling" reflects on a logarithmic scale the product of the SC length and the carrier wavelength. All main effects and interactions were corrected for violations of the sphericity assumption using Box's correction (epsilon or 'ê' in tables; see Keppel, 1991), also reported in ANOVA tables. There were significant main effects of eccentricity and configuration and an interaction of configuration by eccentricity (see Figure 9). Table 4 presents the simple effects or trend analyses of eccentricity and stimulus configuration. Trend analysis found that the Eccentricity effect was mostly linear[15]. Increases in eccentricity were accompanied with increases in scaling at threshold, as expected from the literature. The configuration effect was decomposed in Table 4. When averaged over eccentricities, SC

[14]An 8 (configuration) x 6 (presentation: eccentric and binocular conditions) ANOVA was performed on the full data set to avoid family-wise errors. A main effect of presentation, F (5, 20) = 71.659, p = .0000, and of configuration, F (7, 28) = 40.119, p = .0000, and an interaction, F (35, 140) = 1.877, p = .0055, were observed. Further analyses presented in the text concentrate on theoretically meaningful and systematic sources of variance.

[15]Because the eccentricity levels were not sampled with linear equidistant spacing, this result shouldn't be interpreted as meaning that scaling is a linear function of eccentricity. More appropriate analyses are reported in the "Least-Squares Approach" section below.

discrimination threshold scalings were well-fit by a second degree polynomial in the rotated space as shown by the significant linear and quadratic trends.

Table 4: Simple Effects of Eccentricity or Configuration on Scaling

Source	*df*	MS	F	p
Eccentricity				
Linear	1	48.990	285.751	.0000
Quadratic	1	.365	2.128	.1640
Cubic	1	.381	2.223	.1554
Quartic	1	.002	.010	.9211
Error	16	.171		
Stimulus Configuration (X)				
Linear	1	5.918	171.602	.0000
Quadratic	1	.899	26.070	.0001
Cubic	1	.079	2.299	.1451
Quartic	1	.071	2.057	.1669
Quintic	1	.069	2.008	.1719
Error	20	.034		

Interaction Between Configuration and Eccentricity. The interaction was significant. From this result, it is evident that the curve shape changes with eccentricity. The classic method cannot explain this result. However, an interaction between eccentricity and configuration alone does not necessarily imply that two IMFs influenced task performance. A specific kind of interaction is required for this conclusion to be valid. If two IMFs underlie scaling changes, then the effect would be to shift the rectangular parabola along the configuration axis as well. Because the performance is not linear, it follows that the local slope (Δ scaling / Δ configuration at configuration i) will change with eccentricity of presentation[16]. A slightly less precise test is to fit

[16]The effect is most pronounced where the second derivative has large values, which is near the middle of the rotated rectangular parabola, but very weak near the asymptotic values.

the data at each eccentricity with a line and determine if the slope changes with eccentricity[17]. Following this reasoning, a planned comparison of slope change was constructed. Table 5 shows the weights that test whether the slope of the line that approximates the data changed monotonically across eccentricity conditions. The planned trend comparison of change of slope was significant, $F(1, 80) = 23.751$, $p = .0000$. Therefore, it seems justified to say that two IMFs are required to account for these results.

Table 5: Weights for Slope Change Test

	Configuration (cpa)					
Eccentricity	1	2	4	8	16	32
0.0	-10	-6	-2	2	6	10
2.5	-5	-3	-1	1	3	5
5.0	0	0	0	0	0	0
10.0	5	3	1	-1	-3	-5
20.0	10	6	2	-2	-6	-10

Stimulus-Dependent IMFs. Another perspective on the eccentricity by configuration interaction is that IMFs are stimulus-dependent: when stimulus configuration is changed the relative importance of the limitations imposed by SC length and carrier wavelength vary and so will the IMF. For example, if only a stimulus with 16 cycles per aperture (cpa) was used, the IMF for this configuration might be close to the IMF for carrier wavelength because the task is mostly limited by the visibility of the carrier grating. Indeed, this is what is found, as shown in Figure 10. Edge stimuli (stimuli with less than 1 cpa) are included in Figure 10 to show once again the discontinuity both with the data set and the predictions from measures

[17]This test was done in Pretest 2 (see Appendix B) for one participant. Also, when slope is calculated for each participant for each eccentricity (binocular data counted as well), a within-subjects ANOVA reveals significant slope change, $F(5, 20) = 6.267$, $p = .0012$.

derived using the rectangular parabola (see "Least-Squares Approach" for more details).

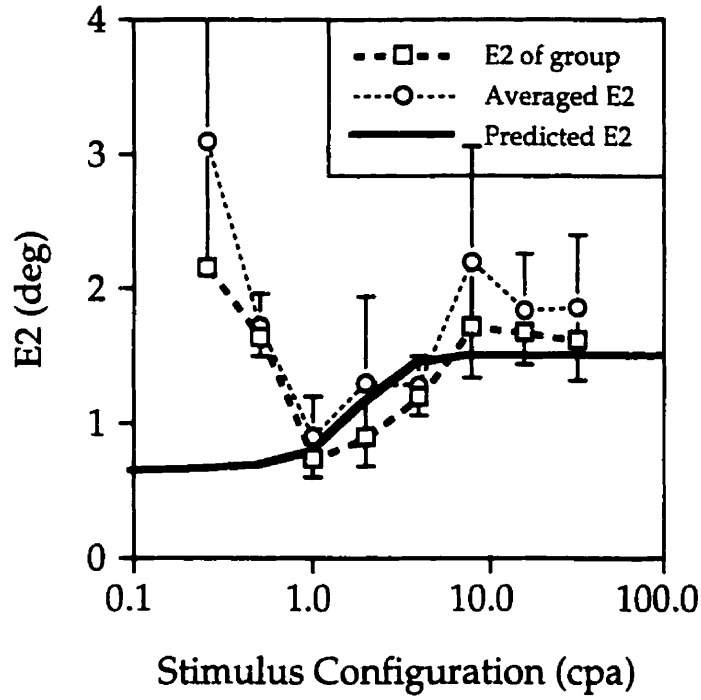

Figure 10. The value of E_2 is stimulus-dependent. E_2 values were calculated in the conventional way (i.e., using the classical method) along each of the eight sampling lines (stimulus configurations). E_2s were calculated for individual subjects and then averaged (circles; error bars represent ± 1 S.E.M.). E_2s were also calculated on the averaged data of the five subjects (squares; without error bars). The thick line plots the predictions of the multiple method calculated on the predictions used with the averaged data. The multiple method provides a good fit the the data above 1 cpa but fails seriously for .25 and .5 cpa. The multiple method provides a good account of eccentricity dependent limitations governing SCs. However, because the .25 and .5 cpa stimuli are categorically different from the SCs one cannot expect them to be governed by the same factors that limit SC discrimination across the visual field.

Least-Squares Approach

Method. ANOVAs have shown that stimulus configuration and eccentricity both influence the scaling threshold, as predicted in Figure 7 and shown in Figure 9. However, to derive specific measures of the mechanisms that encode SCs, a model is required. A model is a set of equations and values that accurately predict the data obtained from participants. For this purpose, a

function describing SC discrimination and another describing eccentricity-dependency were combined. Scaling changed non-linearly with changes in stimulus configuration, and this function can be modelled by the rectangular parabola described by Equations 3, 6 and 7. Scaling increased with eccentricity, a function well-documented in the literature as being linear, i.e. size is a linear function of eccentricity for a wide range of tasks, which is described in Equation 2. In the case of SCs, both SC length and carrier wavelength were assumed to be described by IMFs, as described by Equations 12, 13 and 14. For the rectangular parabola to remain in the same shape in the logarithmic space, the variable ξ^2 was scaled by both IMFs. The model used to predict the scaling for any eccentricity and stimulus configuration is the combination of IMFs and the rectangular parabola, defined by the variables ω, s, ξ, $E_{2\omega}$ and E_{2sc} and described by Equation 14. A least-squares method was used to change the variables until the lowest sum of squared deviations between predicted and actual scaling was reached. The classic method would be identical except for the additional constraint that $E_{2\omega} = E_{2sc}$ as described by Equations 10 and 11.

Data Not Included in the Model. Data for the five participants were fit. Also, the mean scaling was fit and reported as "Group Mean" in Table 6. Data points for binocular viewing were counted as foveal because they were non-significantly different from monocular foveal presentations (see below in the "Binocularity" section). Outliers were removed. It is possible that some luminance edges with .5 cpa may have been encoded as SCs instead, thus cases where the .5 cpa had a higher scaling value than the 1 cpa were treated as if they were processed as SCs, hence were kept in the model. This never happened with the .25 cpa stimuli, i.e. they were always less than one fourth the SC length (aperture size) of the 1 cpa stimuli when the same performance

level was reached. The decision to keep binocular values and some of the .5 cpa conditions was to have as many constraints as possible on the model. Otherwise, some fits were made on too few data points and converged on irrealistic values.

Results. The results of the model fitting are reported in Table 6 and the group's data before and after application of the derived IMFs are shown in Figure 11. The columns of Table 6 present the data set fitted, the characteristics of the foveal rectangular parabola (w_{min}, sc_{min}, ξ; in min of arc), the sc_{min} to w_{min} ratio, the E_2 derived for wavelength and SC length (in degrees), the ratio of E_2s (E_{2w} to E_{2sc}) and the percent variability accounted for by the model (adjusted). The E_2 for wavelength was larger than the E_2 for SC length, $t(4) = 4.655$, $p < .005$[18], supporting again that using only one IMF isn't enough to account for the data.

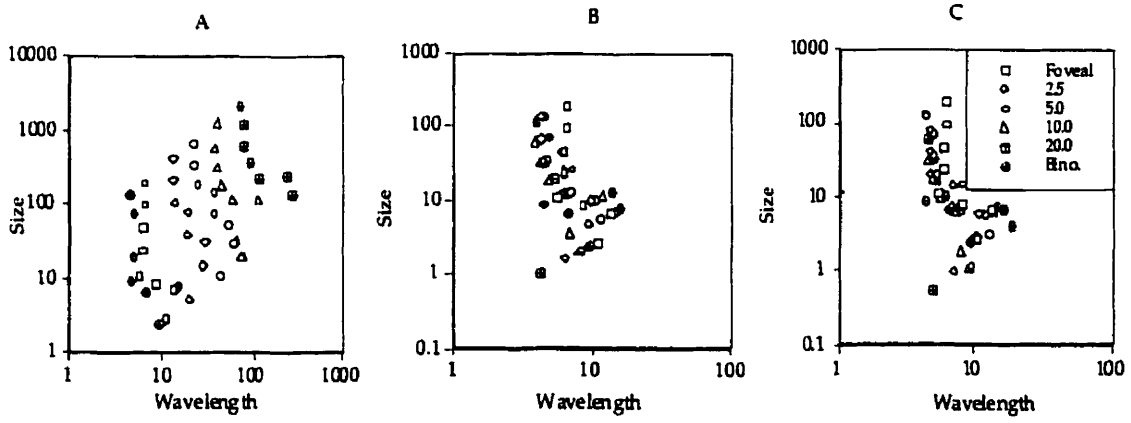

Figure 11. Unscaled and scaled data. (A) Data obtained for 5 participants using the method described in the text. (B) Scaling was done assuming that both axes scale the same way. (C) Scaling done with two IMFs, one for wavelength and one for size. In both scaling methods, the data obtained with stimuli that could not be fit by the rectangular parabola were counted as outliers. Outliers may distort the results, hence were not included in the fit. This occurred often when stimuli had less than 1 cycle per aperture (negative configuration), which causes a break in the function, as depicted in (C). This break in the function is suggesting that these points are detected via a different mechanism than the one encoding the SCs (see text for more details).

[18]It should be noted though that t-tests use less information and are more subject to heterogeneity of variance because E_2 values may not be normally distributed, compared to the ANOVA used above.

Table 6: Data from Individual Curve Fitting

	Model				E_2's			R^2_{adj}
Subjects	w_{min}	sc_{min}	ξ	SC / W	E_{2w}	E_{2sc}	E_{2w} / E_{2sc}	
FP	2.948	6.864	93.754	2.328	1.344	0.655	2.052	95.13%
RG	3.833	6.979	0.342	1.821	1.098	0.449	2.445	97.01%
CP	5.975	10.489	0.000	1.756	3.492	1.912	1.826	93.37%
DR	3.710	9.519	0.000	2.566	1.487	0.950	1.565	92.53%
JK	2.892	3.805	79.791	1.316	1.144	0.254	4.504	98.74%
Mean of S'S	3.871	7.531	34.777	1.957	1.713	0.844	2.479	95.36%
± SEM	0.560	1.169	21.342	0.221	0.450	0.291	0.527	01.14%
Group	3.701	6.087	124.201	1.645	1.479	0.601	2.461	98.74%

Analysis of Residuals. Above is presented a model that was used to derive measures of the mechanisms of SC encoding. "The power of the [model] is reduced to the extent that the [model] cannot map the full extent of the relationship among the [variables]" (Tabachnick & Fidell, 1996, p. 138). To ensure that the model captured all sources of systematic variability or relationships among the variables, ANOVAs were performed on the residuals, that is the difference between measured scaling and predicted scaling (from the fit to the group's data) was used as a dependent variable instead of measured scaling. If the systematic variability in the data was well captured by the model, then evidently the residuals should be randomly distributed at each level of the independent variables. Table 7 presents an ANOVA performed on the residuals of individual participants' response from the model fit to the group means[19]. As in previous ANOVAs, the binocular data and the .25 and .5 cpa data were excluded and the reduced set was analyzed as a 6 (configuration) x 5 (eccentricity) within-subject ANOVA,

[19]Deviations between the data and the individual participant's model could have been used instead. This method would have the effect of greatly reducing the error variance, which would be a more sensitive test but unfortunately would be greatly influenced by outliers. Because the data analyzed are not free of outliers, the former method was preferred.

except where "Full Data Set" is indicated in which case a 8 (configuration) x 6 (eccentricity and binocular foveal) within-subject ANOVA was performed. Table 7 also reports the R^2 values (not adjusted) calculated using the sums of squares of the ANOVAs for comparisons (i.e. $R^2 = (SS_{not\ scaled} - SS_{scaled}) / SS_{not\ scaled}$), which provides a measure of the percent variance of each type (eccentricity, configuration, interaction or slope change) that the model accounted for.

Table 7: Analysis of Residuals: ANOVAs, Simple Effects and R^2s

Source	*df*	SS	MS	F	p	ê	R^2
ANOVA on the Residuals of the Model							
Subjects	4	1.076	.269				
Eccentricity	4	49.697	12.424	72.467	.0000		
Classic	4	.181	.045	.264	.8965		99.27%
Multiple	4	.131	.033	.191	.9397		99.47%
Error	16	2.743	.171			.51	
Configuration	5	7.037	1.407	40.823	.0000		
Classic	5	.278	.056	1.609	.2032		92.25%
Multiple	5	.215	.043	1.245	.3254		93.98%
Error	20	.690	.034			.26	
Interaction	20	1.002	.050	2.063	.0124		
Classic	20	1.001	.050	2.061	.0124		00.10%
Multiple	20	.368	.018	.757	.7544		63.30%
Error	80	1.943	.024			.13	
Planned Comparison of Slope Change							
Reduced Data Set	1		.577	23.751	.0000		
Classic	1		.576	23.731	.0000		00.08%
Multiple	1		.076	3.144	.0800		86.76%
Error	80		.024				
Full Data Set	1		.577	11.776	<.001		
Classic	1		.576	11.755	<.001		
Multiple	1		.076	1.551	>.200		
Error	140		.049				

The classic fit was obtained by assuming that the IMFs for wavelength and SC length were the same, whereas the multiple method used different IMFs. If judged using the absence of main effects in the residuals, both methods provide unbiased accounts of the data. Both methods account for more than 92% and more than 99% of the configuration- and of the eccentricity-dependent variability in the data, respectively. That both models provide a good account of configuration- and eccentricity-dependent variability was expected because the models differed only in the number of IMFs used. However, the classic method accounted for 0.10% and 0.08% of the variability found in the interaction and the slope change test, respectively. This was also expected because the classic method can shift the curve along the scaling axis but not along the stimulus configuration axis. Because a significant interaction remains in the residuals, the model is biased. This failure to reduce the size of the interaction demonstrates the inability of a single IMF to account for all types of variability associated with eccentricity.

In contrast, when the multiple method was used (i.e. two IMFs were used in the model), no significant main effect or interaction was detected, demonstrating the ability of two IMFs to account for all types of variability associated with eccentricity, as shown in Table 7. Indeed, 63.30% and 86.76% of the interaction- and slope change-dependent variability was accounted for by the multiple method respectively. Moreover, the change of slope test did not recover any significant residual variability. The advantage of the multiple method over the classic method is in explaining variability that appears in the form of an interaction between configuration and eccentricity. As seen with simulations, specific interactions arize in cases where two IMFs are required.

Limitations. The data fitting technique used assumed a performance

curve of the form of the rectangular parabola. The rectangular parabola has two asymptotes: one along the SC length and one along the wavelength. However, because the stimulus space is divided in SCs and edges, the data don't asymptote at a minimum SC length. Therefore, the minimum SC length measures are extrapolated, hence subject to substantial measurement error. Consequently, the E_2 for SC length is also extrapolated. The ANOVA does not assume any curve shape, hence is a more objective test of the presence of multiple IMFs.

Other Topics

Binocularity. The 6 (stimulus configuration) x 2 (binocularity) ANOVA revealed neither a main effect, $F(1, 4) = 2.467$, $p = .1914$, nor an interaction of configuration with binocularity, $F(5, 20) = 1.540$, $p = .2225$. The binocular foveal condition was indistinguishable from the monocular foveal condition.

Table 8: Fitting the Edge Data

	E_2s for SCs		Data for Edge		
Subjects	$E_{2\ w}$	$E_{2\ sc}$	Edge	$E_{2\ edge}$	R^2_{adj}
FP	1.344	0.655	2.861	3.202	97.33%
RG	1.098	0.449	3.336	3.174	97.86%
CP	3.492	1.912	3.367	6.938	98.53%
DR	1.487	0.950	3.722	4.818	85.59%
JK	1.144	0.254	1.849	1.889	99.88%
Mean of S'S	1.713	0.844	3.027	4.004	95.84%
SEM	0.450	0.291	0.325	0.868	02.60%
Group	1.479	0.601	3.014	3.694	98.79%

Edges. Because the stimulus space included both edges and SCs, these two stimulus classes were separated in the analyses (recall that the two

stimulus configurations with less than 1 cycle per aperture (cpa) (.25 and .5 cpa, respectively) were defined as luminance egdes). Simple effects were calculated from an 8 (configuration) by 6 (presentation: eccentric and binocular conditions) ANOVA performed on the full data set of 5 participants. Participants were able to discriminate significantly smaller luminance edges than SCs, $F(1, 28) = 142.470$, $p = .0000$. Furthermore, the two luminance edges did not give rise to equivalent performance: .25 cpa stimuli required smaller scaling than .5 cpa stimuli for equivalent performance, $F(1, 28) = 34.947$, $p = .0000$. Table 8 presents the E_2s for SC encoding (for wavelength and SC length), the foveal minimum aperture size for edges (.25 cpa), the E_2 for aperture size and the percent variance accounted for. E_2s for the .25 cpa edges were larger than the E_2s for SC carrier wavelength, $t(4) = 4.564$, $p < .01$. Stimuli with .5 cpa are close to the SC / edge boundary and may engage either or both mechanisms (V1 simple cells and V2 contour cells). This point is further examined in the general discussion and depicted in Figure 12.

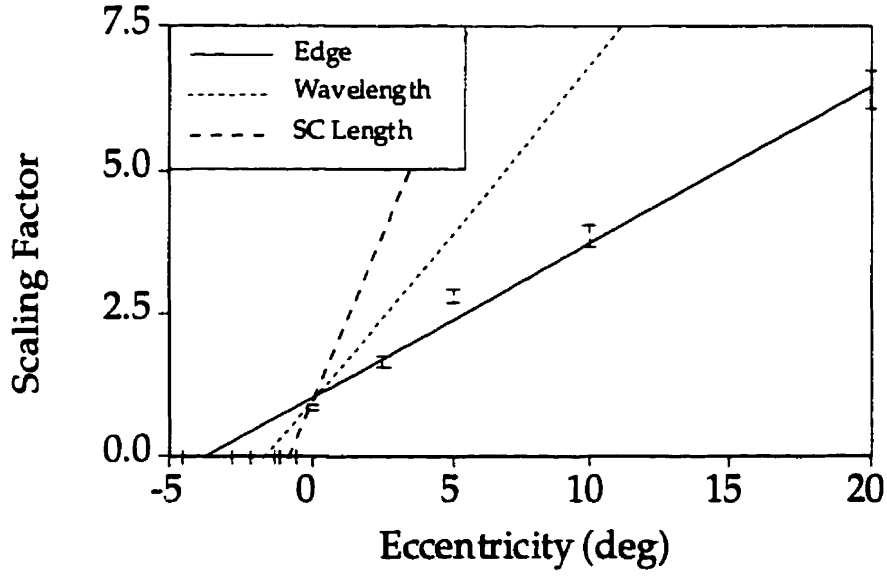

Figure 12. Scaling functions (IMFs). The scaling functions recovered are shown for the SC length

(thick dotted line), the carrier wavelength (thin dotted line) and edges with .25 cpa (full line; vertical error bars show the scaling factors normalized with the foveal predicted value). The functions intersect the x-axis at the value of $-E_2$ (error bars represent S.E.M. of 5 participants).

Individual Differences. From Table 8, it is evident that individual differences in E_2s exist. For example, CP had larger values of E_2s than average. Her E_2 for SC length was larger than E_2s for wavelength of other participants. Similarly, E_2s for edges varied greatly between participants. It is recommended for future experiments on IMFs that several participants be used and that appropriate statistical tests be used to support the conclusions.

Discussion

Summary of Experiment

SCs are thought to be recovered in two stages. Also, sensitivity in most psychophysical tasks changes with eccentricity of presentation. Sensitivity loss can be compensated by scaling the stimuli (applying an IMF). Because the IMF of visual brain areas changes depending on the brain area concerned, it is likely that SCs require at least two IMFs (one per stage) to be equated across eccentricities. The classic method cannot be used to recover multiple IMFs within a task, hence a multiple method was introduced.

The results of the experiment indicate that at least two stages are required to encode SCs. That two IMFs are required to account for SCs was demonstrated in several ways: (1) a paired t-test showed that E_2s recovered for SC length are smaller than for wavelength, also shown in Figure 12, (2) Figure 10 shows that IMFs were configuration-dependent, (3) the ANOVA showed an interaction, which was further analyzed by a slope change test, and (4) the interaction and slope change were accounted for only when two IMFs

were used in the model. These results are inconsistent with views that a given task requires only one IMF to be equated throughout peripheral vision. Also, simple luminance edges were much less limited by eccentricity of presentation than SCs, as demonstrated with paired t-tests between E_2s for .25cpa edges and for SC carrier wavelength, also shown in Figures 10 and 12. The experiment permitted to recover three significantly different IMFs: from shallowest to steepest they account for edges, SC carrier wavelength and SC length.

Some considerations were raised concerning experiments that attempt to recover IMFs associated with different tasks. The classic way of calculating E_2 assumes that a task can be described with only one IMF. This considerably reduces variability in the data. However, careful examination of the present data revealed other sources of variability that the classic method cannot explain. This small but systematic variability is critical in developing models of SC discrimination. These sources of variability may not be apparent to the eye but can be readily recovered by appropriate statistical analyses. The error of assuming that only one IMF underlies task performance changes with eccentricity reveals an E_2 that is a weighted average of all underlying E_2s, and other values extracted through modelling can be erroneous as well.

The multiple method, based on visual limits, can independently measure different axes' magnification with eccentricity. Also, the rectangular parabola isn't limited to measuring two limits as it can be used to describe tasks that are limited by 3 or 4 dimensions. Moreover, the rotation in log space permits one to treat the stimulus configuration (X) as an independent variable and the scaling (Y) as a dependent variable. This permits the coherent and structured sampling of the data space and the use of statistical techniques such as ANOVAs, multiple regression or modelling to assess data

that were previously difficult to interpret. Without the use of appropriate statistical methods, experimenters always run the risk of seeing what they expect to see in the data. This problem is particularly serious when only a small difference in variance leads to a large difference in theory.

Acuity of Processing Stages

Wavelength (ω_{min}). To compare the measures of acuity to other experiments, the derived minimum wavelength is compared to grating acuity and the derived minimum size is compared to general hyperacuity results. Foveally, SCs cannot be resolved on carriers with wavelengths smaller than 3.871±0.560′ arc (≈ 15.50 cpd) even when the aperture is relatively large (≈ 20′ arc). These values are slightly larger than the typical human range of grating acuity, which ranges from 38″ to 120″ arc (≈30 to ≈95 cpd) (Rovamo & Virsu, 1979; Virsu et al., 1987; Thibos et al., 1996). The E_2 derived for carrier wavelength in the present experiment was 1.713°±0.450°, which is similar to E_2s for acuity tasks like Snellen acuity (Virsu et al., 1987), geometric distortions (Rovamo et al., 1997), T resolution (Toet & Levi, 1992) and the center region of end-stopped mechanisms (Yu & Essock, 1996). However, the E_2 for wavelength in our task is smaller than in grating acuity tasks (Rovamo & Virsu, 1979; Virsu et al., 1987; Thibos et al, 1996). The fact that a longer wavelength has to be present both in the fovea and in the periphery than in conventional grating acuity tasks is readily understood because two gratings are superimposed, causing some interference in the signal. Furthermore, the mechanism that mediates SC discrimination is not the one that mediates grating detection. Therefore, there is no reason to expect the E_2 for the carrier wavelength dimension of the present stimuli to be equal to the E_2 for grating acuity.

SC Length (s_{min}). SCs have to be at least 7.531±1.169′ arc long for discrimination at threshold when the carrier grating's wavelength is large enough to be clearly seen (≈ 10′ arc). IMFs for texture boundaries are scarce in the literature for comparison. However, hyperacuity tasks have been investigated. Hyperacuity tasks are tasks where acuity is better than predicted by cone density. It is hypothesized that V1 cell responses are pooled for increase of accuracy (for example, see Paradiso, 1988), similarly to SCs. For this reason, minimum SC length should lie in the ranges of minimum lengths required in other hyperacuity tasks. However, this value is somewhat larger than minimum line lengths for orientation, curvature, displacement and bisection acuity tasks, which are in the range of 1.49′ to 3′ (Mäkelä et al., 1993; Whitaker, Mäkelä et al., 1993, Whitaker, Rovamo et al., 1992; Virsu et al., 1987). The SC was created by a texture edge, unlike most other acuity and hyperacuity tasks which were constructed with line elements and dots. For this reason, if a similar mechanism is used for texture segregation and hyperacuity, it would require more integration surface for textures than for line elements and dots. The E_2 for SC length was 0.844°±0.291°, a steeper figure when compared to hyperacuities such as vernier acuity, orientation discrimination and curvature (Whitaker, Rovamo et al., 1992; Virsu et al., 1987; Mäkelä et al., 1993; Whitaker, Mäkelä et al., 1992).

This is not surprising. The present experiment has separated the different levels of resolution. Other studies of hyperacuity have not explicitly separated performance loss due to resolution of the target versus limitations due to the task *per se* (Mäkelä et al., 1993; Virsu et al., 1987; Whitaker, Latham, Mäkelä & Rovamo, 1993; Whitaker, Mäkelä et al., 1992; Whitaker, Rovamo et al., 1992). For example, curvature detection can be limited by resolution of the stimuli and by the amount of curvature. For this reason, the

E_2 recovered could represent resolution of the target, limitations of the "hyperacuity" cells or some combination of the two. Without appropriate analyses, these studies cannot claim to have precisely recovered the E_2 for the hyperacuity task.

Multiple IMFs

Very few studies have been specifically concerned with whether two or more E_2s might mediate performance in a task. The only studies of this sort concern two-dot vernier acuity (Westheimer, 1982), spatial interval discrimination (Levi & Klein, 1990; Yap, Levi & Klein, 1989) and end-stopped mechanisms (Yu & Essock, 1996).

Hyperacuities. Westheimer (1982) varied the vertical separation (vs) between two dots and determined the minimum or threshold horizontal separation (th) required for right-oblique versus left-oblique discrimination for several eccentricities. Scaling was measured along these two dimensions, and it was found that more than one IMF was required to make the curves overlap. Westheimer's task may be seen as an orientation discrimination task, which suggests the involvement of orientation-selective simple cells in V1, or other orientation-selective cells elsewhere in the visual system. For this reason, it seems reasonable to quantify stimulus characteristics by the orientation and the length (i.e. the distance between the two dots) rather than vertical and horizontal separation. This would entail the transformation from vertical separation (vs) and horizontal separation (or threshold: th) to the distance between the dots ($=[vs^2 + th^2]^{0.5}$) and the orientation of the dots (=atan [th/vs]). It is evident that the IMFs recovered by Westheimer (1982) would not apply to these new axes. It is difficult, however, from his results to calculate what the appropriate IMFs would be. This would require the

transformation of the data from threshold and vertical separation to orientation and length prior to the scaling operation. If length and orientation are really the relevant dimensions in Westheimer's task, then the derived E_2s are probably only indirectly related to physiological properties that mediate the task. The appropriate E_2 should be similar to the E_2 derived by Mäkelä et al. (1993).

End-Stopped Cells. Yu and Essock (1996) investigated eccenticity-dependent changes in the structure of end-stopped mechanisms. This is of particular interest to the present research because end-stopped cells have been used in some models of SC encoding (Peterhans & von der Heydt, 1991; Grinberg, 1994; Gurnsey et al., 1992; Gurnsey et al., submitted).

Yu and Essock (1996) assumed some qualitative receptive field characteristics of end-stopped cells throughout their study, although these characteristics were not formally defined. The receptive field structure presented in Figure 13A includes three regions. The center region is excitatory and elongated. The flank regions are also elongated but they are inhibitory. Finally, the end-stopped regions are vaguely defined in shape but are inhibitory in nature. In short, such cells respond optimally to bars of a particular width, length and orientation.

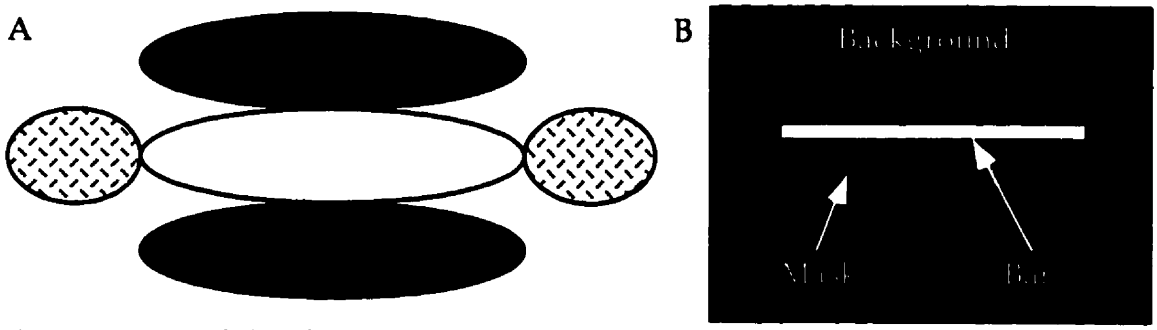

Figure 13. Yu and Essock's experiment (1996). (A) Proposed receptive field structure of end-stopped cells. The center region (white) is excitatory and the flank regions (black) are inhibitory. Also, end-stopped regions (textured) on both ends of the cell's receptive field inhibit the cell's response if the stimulus within the cell's center region extends beyond the

excitatory region. In short, the cell prefers a bar of a certain width, length and orientation. (B) The stimulus presented to participants was a line superimposed on a rectangle of variable dimensions. The luminance difference between the background and the rectangle was constant while the luminance difference between the bar and the rectangle was varied to determine threshold performance.

Yu and Essock (1996) presented a bar on a background of a fixed luminance and measured the luminance increment required to detect the bar. The task was repeated for cases when the bar was superimposed on a mask rectangle of different dimensions, as shown in Figure 13B, and the luminance increment thresholds were measured. Sensitivity to a luminance increment of the bar is assumed to be lowest when the rectangular mask fills the center region but doesn't exceed it. Also, sensitivity should be independent of the mask's dimensions as long as the mask fully overlaps the receptive field of the end-stopped cell, i.e. when it completely covers the center, flank and end-stopped regions. Using the peaks and plateaus of the luminance increment threshold curves, Yu and Essock (1996) measured the sizes of the different regions at several eccentricities. They concluded that the end-stopped, flank and center regions all scale at different rates (E_2s = .45, .77 and 2.05 respectively).

In relating their results to ours, several difficulties arise. Firstly, it is difficult to imagine how their mechanism would respond to our stimuli. Secondly, end-stopped models of SC encoding usually use a second layer of cells to encode the co-alignment of end-stopped cells that respond strongly. Yu and Essock (1996) did not investigate if such a second layer existed. Thirdly, our stimuli comprised two superimposed gratings with a phase shift. The end-stopped receptive field structure presented in Figure 13A is specialized to encode lines of a certain length and width. Because center and flank regions are not always of equal size, the description of stimuli in terms

of wavelengths is incompatible with end-stopped mechanisms modeled by Yu and Essock (1996) which would prefer gratings that are composed of thinner white lines and larger black lines. It is evident that much more work needs to be done if a connection between end-stopped cells and the present results of SC encoding is to be made.

A Revised Model of the Perception of SCs

Biological Substrates. The two dimensions studied in the present research were selected to represent receptive field properties of cells in the visual cortex. The first layer of cells, associated with V1 simple cells, are differently stimulated by gratings of different wavelengths. Similarly, the second layer of cells, associated with V2 contour cells, are responsive to SCs within their receptive field. Hence, to measure properties of the two layers of cells, wavelength and SC length were manipulated. The results of the present experiment do not preclude the presence of other levels of processing. For example, it is possible that an intermediary end-stopped layer of cells spatially sharpened the responses before the V2 cells encoded the SC. However, by finding the IMFs of two rather than just one limiting dimension, our findings are more likely to represent characteristics of biological substrates, unless a third E_2 plays a role in the task. Unfortunately, precise measurements of E_2 for human biological substrates are still not available for comparison.

On the Revised Model of SC Encoding

The first stage would be limited by wavelength-selectivity in V1 simple cells, proposed to be roughly proportional to cone or retinal ganglion cell density or receptive field size in V1 simple cells, because these substrates are

thought to limit the minimum distance between two lines resolveable. Accordingly, the IMF for wavelength was close but somewhat steeper than IMFs for grating acuity (1.713 in the present experiment compared to values from 2.38 to 4.14; see Table 1). Little is known about the properties of cells in V2, but if SC length correctly reflects the receptive field size of V2 contour cells, then E_2 for V2 receptive field size is in the range of cortical magnifications (0.844 in the present experiment compared to values from 0.3 to 1.237; see Table 1).

Wilson and Richards' Model. Wilson and Richards (1992) proposed a two-layer filter model to explain the encoding of curvature defined with SCs. The first layer of filters have the properties of V1 simple cells. The responses of these filters are rectified and serve as input to a second layer filter. Wilson and Richards proposed that the second layer filters should be twice the scale of the first layer filters. The model proposed by Wilson and Richards (1992) must be modified to account for our results because SC length scales faster with eccentricity than carrier wavelength. The ratio of second to first layer size cannot be estimated here unless a ratio of receptive field size to preferred wavelength is assumed for the first layer filters. Nevertheless, the ratio of minimum SC length to minimum wavelength is used for comparison ($R(e) = sc_{min} / \omega_{min}$; see Table 6). The "foveal" ratio is 1.957±.221. This ratio should be a multiple constant away from the actual ratio of second to first layer receptive field size used by Wilson and Richards (1992). The ratio R(e) changes as a function of eccentricity, given by:

$$R(e) = Rf\,(1 + e / E_{2sc}) / (1 + e / E_{2\omega}), \text{ and} \qquad \text{[Eq 16]}$$

$$R(e) \approx Rf\,E_{2\omega} / E_{2sc}, \text{ when } e >> 0, \qquad \text{[Eq 17]}$$

where Rf is the "foveal" ratio. At very large eccentricities (> 15°), this ratio is approximated by Equation 17 and equals 4.473±.706, which is about 2.3 times larger than the foveal value. If Wilson and Richards' estimate of the ratio of second to first layer is accurate for foveal viewing, then it should be about 4.6 for peripheral viewing (>15°). This means that more line endings would be required for a SC to be perceived with the same salience, even when spatial frequency has been adjusted with the first stage's sampling characteristics. The relationship between the ratio of sc_{min} to ω_{min} and eccentricity is shown in Figure 14. It is interesting to note in Figure 14 that the greatest change of ratio occurs within 0.1° and 10°.

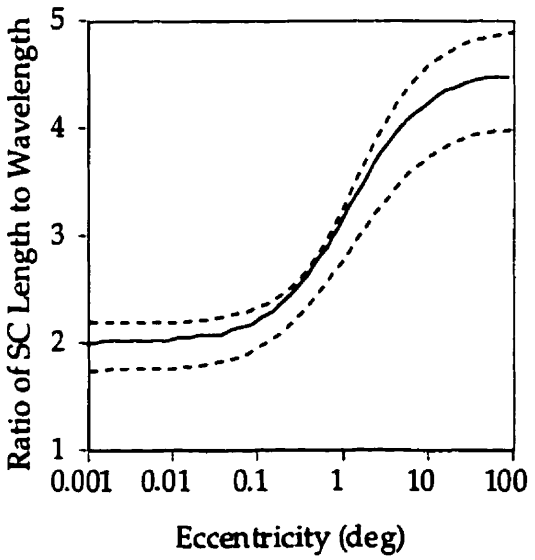

Figure 14. Eccentricity-dependence of SC length to wavelength ratio. The ratio was calculated for different eccentricities for the five participants using Equation 15. The dark line represents the average, and the dotted line represents the S.E.M. The greatest change of ratio occurs between 0.1° and 10° of eccentricity.

"Back-Pocket" Models. In the two-stage model presented above, the grating used for simulations was perpendicular to the SC. It is clear however that participants could integrate oblique gratings to form a percept of a SC despite the non-orthogonality of the SC and the gratings. Alternatively, SCs

defined by orientation, wavelength, contrast or other attributes could have been detected by a similar model. Indeed, in cases of texture edges a percept of a SC appears, even though the attribute used to create the percept isn't necessarily a phase shift. A general model could integrate across many orientations and wavelengths and therefore be expected to "perceive" several types of SCs or texture boundaries. A second layer quadrature pair could be used so that the percept of a SC can be due either to a drop of response on the SC (as is the case when a phase shift occurs) or a change in response across the SC (as is the case when an orientation contrast is present, for example).

Indeed, several models in texture segregation involve two stages of processing with some non-linearity between the two stages to encode the texture gradients (Bergen & Landy, 1991; Caelli, 1985; Fogel & Sagi, 1989; Griffiths & Troscianko, 1991; Gurnsey & Browse, 1989; Landy & Bergen, 1991; Malik & Perona, 1990; Vogels & Orban, 1987; Wilson & Richards, 1992; Wolfson & Landy, 1995). These models have been so widely used that Chubb and Landy (1991) referred to them as "Back-Pocket Models", "as researchers routinely pull these models out of their back pockets to explain new results in texture segregation" (Wolfson & Landy, 1995, p.2864). Given the similarities of these models and the one used in this research, it is likely that the mechanisms used to encode the perceptual edge are the same, whether it is caused by a phase shift, an orientation contrast or other type of discontinuity. From this point of view, it is possible that our IMFs apply to most if not all of the cases where "Back-Pocket" models have been successfully applied. However this remains to be tested.

Binocular Integration. Edges caused by texture differences are thought to be extracted after binocular integration (Frisby & Mayhew, 1979). Surprisingly, binocular integration had no significant effect on the detection of SCs. It is interesting, however, that most participants reported that the binocular viewing condition was easier than the monocular viewing

condition. Participants probably preferred the binocular viewing condition because it is unusual to view the world monocularly. Regarding performance changes, binocular integration usually requires time to occur, and it is likely that not enough time was given for performance to improve significantly. If the binocular viewing condition had yielded smaller minimum grating wavelength or smaller minimum SC length, the locus of integration could have been associated with the V1 or V2 cells. However, in the absence of an effect, it is difficult to conclude anything regarding the locus of integration with the SC model or the Back-Pocket models.

Locus of Integration. If it is assumed that texture differences are extracted after binocular integration as suggested by Frisby and Mayhew (1979) and that the perception of SCs is a specialized case of texture perception, then either binocular integration occurs before the first stage or between the two stages. To assess whether the binocular integration occurs before or after the first stage of SC perception, a stimulus giving different predictions is created. In Figure 15, the gratings seem to integrate into an unbroken grating. Nevertheless, a SC percept emerges even though no clear reason for its appearance is evident. If integration occurred before or at the level of the first layer filters, the SC would not give rise to response changes and would not be encoded. However, if binocular integration occurs after the first layer of filters, the response drop occurs and the SC is still encoded.

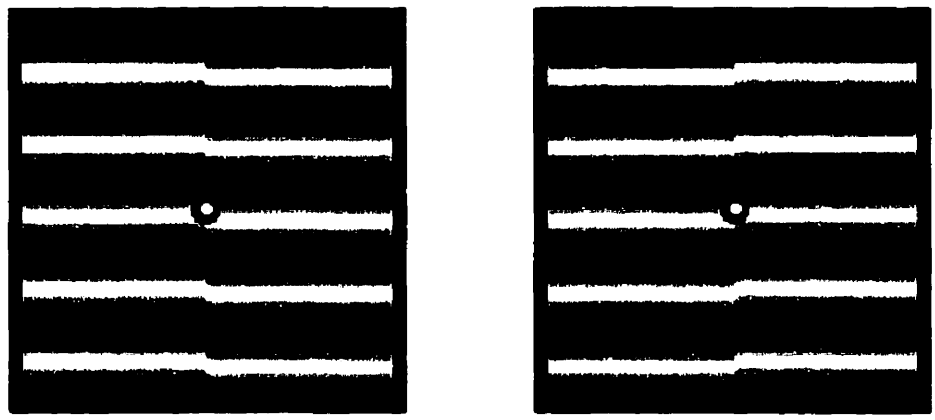

Figure 15. Binocular display of SC. When these two displays are integrated, participants

report seeing a clear vertical contour in the middle. For this percept to arise, it is necessary that a response discontinuity occurs at the locus of the SC before binocular integration occurs. However, participants also report that the two textures do not appear phase-shifted relative to each other or in any other way different. The fact that the textures don't appear different suggests that the texture boundary is computed from information that is lost when binocular integration occurs, but nevertheless the information of the presence of a boundary is kept. However, the percept could also be explained with binocular rivalry (see text for more details).

This suggests that the binocular integration occurs at least after the first layer of filters. Studies of V1 simple cells agree with this speculation. DeAngelis et al. (1991) proposed that binocular simple cells in V1 may have phase differences between the right and left eye's input, making them sensitive to disparity. However, many simple cells in V1 are monocular, which would be sufficient for a drop in response to occur at the location of the SC. Complex cells could then pool information to recover depth information. Because the SC is recoverable from monocular V1 cells, a contour may be detected in subsequent layers.

However, the percept can also occur if binocular rivalry occurs locally, leaving enough information to the cyclopean view to create a SC percept. This is indeed what some participants reported. Therefore, further work is needed before the locus of integration is accepted regarding the Back-Pocket models. So far, only the specific tests of eccentricity and stimulus configuration as presented above give a reliable demonstration that two stages exist to encode SCs.

Alternative Theory. Alternative explanations of SC encoding are also possible while remaining consistent with the present results. It is possible that while the V1 simple cell's receptive field size and wavelength selectivity correctly correspond to wavelength scaling properties, the V2 cell's receptive field size may be incorrectly represented by our model. Indeed, if it is assumed that scaling is approximately the same for receptive field size of cells

throughout the cortical visual areas, then the SC length scaling would require another explanation. It is known that receptive field and cortical magnification in V1 do not scale at the same rate (Dow et al., 1981). Consequently, if V2 cells' receptive fields are proportional to V1 cells' receptive fields in size, it is likely that V2 integrate their responses from more V1 cells when their receptive fields fall in the foveal region. Hence, it is expected that the signal to noise ratio is better for V2 foveal cells than V2 peripheral cells. Compensation for signal-to-noise loss in the periphery is achieved by stimulating more cells, i.e. stimulating a larger area of the retina. By this theory, the number of cells stimulated in V1 by a given stimulus would be critical in determining performance in a task involving SCs. It is evident that more work is required to distinguish between this possibility and other variations on the model. However, it is clear that two sources of limitations are influencing task performance, and any model proposed to account for our results will have to include two sources of limitation that have different IMFs.

References

Azzopardi, P., & Cowey, A. (1993). Preferential representation of the fovea in the primary visual cortex. Nature, 361, 719-721.

Baseler, H.A., & Sutter, E.E. (1997). M and P components of the VEP and their visual field distribution. Vision Research, 37 (5), 675-690.

Bergen, J.R., & Landy, M.S. (1991). Computational modeling of visual texture segregation. In M.S. Landy & J.A. Movshon. (Eds.), Chapter 17: Computational Models of Visual Processing (pp. 253-271). Cambridge, MA: MIT Press.

Bennett, P.J., & Banks, M.S. (1987). Sensitivity loss in odd-symmetric mechanisms and phase anomalies in peripheral vision. Nature, 326, 873-876.

Bradley, A., Skottun, B. C., Ohzawa, I., Sclar, G., & Freeman, R. D. (1985). Neurophysiological evaluation of the differential response model for orientation and spatial-frequency discrimination. Journal of the Optical Society of America A., 2 (9), 1607-1610.

Bradley, A., Skottun, B.G., Ohzawa, I., Sclar, G., & Freeman, R.D. (1987). Visual orientation and spatial frequency discrimination: a comparison of single neurons and behavior. Journal of neurophysiology, 57 (3), 755-772.

Burr, D.C., Morrone, M.C., & Spinelli, D. (1989). Evidence for edge and bar detectors in human vision. Vision Research, 29 (4), 419-431.

Caelli, T. (1985). Three processing characteristics of visual texture segmentation. Spatial Vision, 1 (1), 19-30.

Carrasco, M., & Frieder, K.S. (1997). Cortical magnification neutralizes the eccentricity effect in visual search. Vision Research, 37 (1), 63-82.

Chubb, C., & Landy, M.S. (1991). Orthogonal distribution analysis: A

new approach to the study of texture perception. In Landy, M.S. & Movshon, J.A. (Eds.), Chapter 19: Computational Models of Visual Processing (pp. 291-301). Cambridge, MA: MIT Press.

DeAngelis, G.C., Freeman, R.D., & Ohzawa, I. (1994). Length and width tuning of neurons in the cat's primary visual cortex. Journal of Neurophysiology, 71, 347-374.

DeAngelis, G.C., Ohzawa, I., & Freeman, R.D. (1991). Depth is encoded in the visual cortex by a specialized receptive field structure. Nature, 352, 156-159.

DeValois, R.L., Albrecht, D.G., & Thorell, L.G. (1982). Spatial frequency of cells in macaque visual cortex. Vision Research, 22, 545-559.

Dow, B.M., Snyder, A.Z., Vautin, R.G., & Bauer, R. (1981). Magnification factor and receptive field size in foveal striate cortex of the monkey. Experimental Brain Research, 44, 213-228.

Fogel, I., & Sagi, D. (1989). Gabor filters as texture discriminator. Biological Cybernetics, 61, 103-113.

Francis, G., & Grossberg, S. (1996). Cortical dynamics of form and motion integration: persistence, apparent motion, and illusory contours. Vision Research, 36(1), 149-173.

Frisby, J.P., & Mayhew, J.E.W. (1979). Does visual texture discrimination precede binocular fusion? Perception, 8, 153-156.

Goldstein, E.B. (1996). Sensation & Perception. Pacific Grove, CA, Brooks/Cole Publishing.

Griffiths, E., & Troscianko, T. (1991). Can human texture discrimination be mimicked by a computer model using local Fourier analysis?. Spatial Vision, 6 (2), 149-157.

Grinberg, D.I. (1994). Discrimination of subjective contours defined by

offset gratings: effects of contour length, inter-line spacing, and regularity of spacing. Unpublished manuscript, Concordia University, Montréal, Québec, Canada.

Gurnsey, R., & Browse, R.A. (1989). Asymmetries in visual texture discrimination. Spatial Vision, 4 (1), 31-44.

Gurnsey, R., Humphrey, G.K., & Kapitan, P. (1992). Parallel discrimination of subjective contours defined by offset gratings. Perception and Psychophysics, 52 (3), 263-276.

Gurnsey, R., Iordanova, M., & Grinberg, D. (1997). Detection and discrimination of subjective contours defined by offset gratings. Manuscript submitted for publication.

Grosof, D.H., Shapley, R.M., & Hawken, M.J. (1993). Macaque V1 neurons can signal 'illusory' contours. Nature, 365 (7), 550-552.

Grüsser, O.J. (1995). Migraine phosphenes and the retino-cortical magnification factor. Vision Research, 35(8), 1125-1134.

Hays, W.L. (1926). Basic Statistics. Belmont, CA: Brooks/Cole Publishing.

von der Heydt, R., & Peterhans, E. (1989). Mechanisms of contour perception in monkey visual cortex: I. Lines of pattern discontinuity. Journal of Neuroscience, 9 (5), 1731-1748.

von der Heydt, R., Peterhans, E., & Baumgartner, G. (1984). Illusory contours and cortical neuron responses. Science, 224, 1260-1262.

Hirsch, J., & Curcio, C.A. (1989). The spatial resolution capacity of human foveal retina. Vision Research, 29 (9), 1095-1101.

Horton, J.C., & Hoyt, W.F. (1991). The representation of the visual field in human striate cortex. Archives of Ophthalmology, 109, 816-824.

Hubel, D. (1996). A big step along the visual pathway. Nature, 380 (21),

197-198.

Hubel, D.H., Wiesel, T.N., & Stryker, M.P. (1978). Anatomical demonstration of orientation columns in macaque monkeys. Comparative Neurology, 177, 361-380.

Hubel, D.H., & Wiesel, T.N. (1974a). Sequence Regularity and Geometry of Orientation Columns in the Monkey Striate Cortex. Journal of Comparative Neurology, 158, 267-294.

Hubel, D.H., & Wiesel, T.N. (1974b). Uniformity of Monkey Striate Cortex: A Parallel Relationship between Field Size, Scatter, and Magnification Factor. Journal of Comparative Neurology, 158, 295-306.

Keppel, G. (1991). Design and Analysis: A Researcher's Handbook (3rd Ed.). Englewood Cliffs, NJ: Prentice Hall.

Landy, M.S., & Bergen, J.R. (1991). Texture segregation and orientation gradient. Vision Research, 31 (4), 679-691.

Levi, D.M., Klein, S.A., & Aitsebaomo, A.P. (1985). Vernier acuity, crowding and cortical magnification. Vision Research, 25 (7), 963-977.

Levi, D.M., & Klein, S.A. (1990). Equivalent blur in spatial vision. Vision Research, 30 (12), 1971-1993.

Lieberman, H.R., & Pentland, A.P. (1982). Microcomputer-based estimation of psychophysical thresholds: The BEST PEST. Behavior, Research Methods & Instrumentation, 14 (1), 21-25.

Madigan, R., & Williams, D. (1987). Maximum-likelyhood psychometric procedures in two-alternative forced-choice: Evaluation and recommendations. Perception and Psychophysics, 42 (3), 240-249.

Mäkelä, P., Whitaker, D., Rovamo, J. (1993). Modelling orientation discrimination across the visual field. Vision Research, 33 (5), 723-730.

Malik, J., & Perona, P. (1990). Preattentive texture discrimination with

early vision mechanisms. Optical Society of America, 7 (5), 923-932.

Marcelja, S. (1980). Mathematical Description of the Responses of Simple Cortical Cells. Journal of the Optical Society of America, 70 (11), 1297-1300.

Morrone, M.C., Burr, D.C., & Spinelli, D. (1989). Discrimination of Spatial Phase in Central and Peripheral Vision. Vision Research, 29 (4), 433-445.

Mulligan, K., & Sherk, H. (1993). A Comparison of Magnification Functions in Area 19 and the Lateral Suprasylvian Visual Area in the Cat. Experimental Brain Research, 97, 195-208.

Orban, G.A., Kato, H, & Bishop, P.O. (1979). End-zone region in the receptive fields of hypercomplex and other striate neurons in the cat. Journal of Neurophysiology, 42, 818-832.

Paradiso, M.A. (1988). A theory for the use of visual orientation information which exploits the columnar structure of striate cortex. Biological Cybernetics, 58, 35-49.

Paradiso, M. A., & Carney, T. (1988). Orientation discrimination as a function of stimulus eccentricity and size: nasal/temporal retinal asymmetry. Vision Research, 28 (8), 867-874.

Pentland, A. (1980). Maximum likelihood estimation: the Best PEST. Perception and Psychophysics, 28 (4), 377-379.

Peterhans, E., & von der Heydt, R. (1991). Subjective contours: Bridging the gap between psychophysics and physiology. Trends in Neurosciences, 14 (3), 112-119.

Poirier, F.J.A.M., & Gurnsey, R. (1996). The effect of eccentricity and spatial frequency on orientation discrimination asymmetries. Investigative Ophthalmology and Visual Science, 37 (3), S295.

Poirier, F.J.A.M., & Gurnsey, R. (1997). The effect of eccentricity and spatial frequency on orientation discrimination asymmetries. Manuscript submitted for publication.

Pollen, D.A., & Ronner, S.F. (1981). Phase relationships between adjascent simple cells in the visual cortex. Science, 212 (19), 1409-1411.

Pollen, D.A., & Ronner, S.F. (1982). Spatial computation performed by simple and complex cells in the visual cortex of the cat. Vision Research, 22, 101-118.

Pollen, D.A., & Ronner, S.F. (1983). Visual Cortical Neurons as Localized Spatial Frequency Filters. IEEE Transactions on Systems, Man, and Cybernetics, 13 (5), 907-916.

Rolls, E.T., & Cowey, A. (1970). Topography of the retina and striate cortex and its relationship to visual acuity in rhesus monkeys and squirrel monkeys. Experimental Brain Research, 10, 298-310.

Rovamo, J., Mäkelä, P., Näsänen, R., & Whitaker, R. (1997). Detection of geometric image distortions at various eccentricities. Investigative Ophthalmology and Visual Science, 38 (5), 1029-1040.

Rovamo, J., & Virsu, V. (1979). An Estimation and Application of the Human Cortical Magnification Factor. Experimental Brain Research, 37, 495-510.

Rovamo, J., Virsu, V., & Näsänen, R. (1978). Cortical magnification factor predicts the photopic contrast sensitivity of peripheral vision. Nature, 271(5), 54-56.

Scobey, R. P. (1982). Human Visual Orientation Discrimination. Iounal of Neurophysiology, 48 (1), 18-26.

Sereno, M.I., Dale, A.M., Reppas, J.B., Kwong, K.K., Belliveau, J.W., Brady, T.J., Rosen, B.R., & Tootell, R.B.H. (1995). Borders of multiple visual

areas in humans revealed by functional magnetic resonance imaging. Science, 268, 889-893.

Serway, R.A. (1992). Physics For Scientists & Engineers with Modern Physics (3rd Ed.). Orlando, FL: Harcourt Brace Jovanovich.

Simpson, W.A. (1989). The step method: A new adaptive psychophysical procedure. Perception and Psychophysics, 45 (6), 572-576.

Smith, E. L., Chino, Y. M., Ridder, W. H., Kitagawa, K., & Langston. (1990). Orientation Bias of Neurons in the Laterate Geniculate Nucleus of Macaque Monkeys. Visual Neuroscience, 5 (6), 525-545.

Soriano, M., Spillman, L., & Bach, M. (1996). The abutting grating illusion. Vision research, 36 (1), 109-116.

Tabachnick, B.G., & Fidell, L.S. (1996). Using Multivariate Statistics. (3rd Ed.). New York, NY: HarperCollins.

Thibos, L.N., Still, D.L., & Bradley, A. (1996). Characterisation of spatial aliasing and contrast sensitivity in peripheral vision. Vision Research, 36 (2), 249-258.

Toet, A., & Levi, D.M. (1992). The two-dimensional shape of spatial interaction zones in the parafovea. Vision Research, 32 (7), 1349-1357.

Ungerleider, L.D., & Mishkin, M. (1982). Two cortical visual streams. In Ingle, D.J., Goodale, M.A., & Mansfield, R.J.W. (Eds.), Analysis of Visual Behavior, (pp.549-585). Cambridge, MA: MIT Press.

Virsu, V., Näsänen, R., & Osmoviita, K. (1987). Cortical magnification and peripheral vision. Journal of the Optical Society of America A, 4 (8), 1568-1578.

Virsu, V., Rovamo, J., Laurinen, P., & Näsänen, R. (1982). Temporal Contrast Sensitivity and Cortical Magnification. Vision Research, 22, 1211-

1217.

Vogels, R., & Orban, G.A. (1987). Illusory contour orientation discrimination. Vision Research, 27(3), 453-467.

Watson, A.B. (1987). Estimation of local spatial scale. Journal of the Optical Society of America A., 4 (8), 1579-1582.

Watson, A.B., & Pelli, D.G. (1983). QUEST: A Bayesian adaptive psychometric method. Perception and Psychophysics, 33 (2), 113-120.

Weymouth, F.W. (1958). Visual sensory units and the minimal angle of resolution. American Journal of Ophthalmology, 46, 102-113.

Westheimer, G. (1982). The spatial grain of the perifoveal visual field. Vision Research, 22, 157-162.

Whitaker, D., Latham, K., Mäkelä, P., & Rovamo, V. (1993). Detection and discrimination of curvature in foveal and peripheral vision. Vision Research, 33 (16), 2215-2224.

Whitaker, D., Mäkelä, P., Rovamo, J., & Latham, K. (1992). The Influence of Eccentricity on Position and Movement Acuities as Revealed by Spatial Scaling. Vision Research, 32 (10), 1913-1930.

Whitaker, D., Rovamo, J., MacVeigh, D., & Mäkelä, P. (1992). Spatial scaling of vernier acuity tasks. Vision Research, 32 (8), 1481-1491.

Wilson, H.R., Levi, D., Maffei, L., Rovamo, J., DeValois, R. (1990). The perception of form: Retina to striate cortex. In Spillmann, L., & Werner, J. S. (Eds.), Visual Perception: The Neurophysiological Foundations, (pp.231-271). San Diego, CA: Academic Press, Inc.

Wilson, H.R., & Richards, W.A. (1992). Curvature and Seperation Discrimination at Texture Boundaries. Journal of the Optical Society of America A, 9 (10), 1653-1661.

Wolfson, S.S., & Landy, M.S. (1995). Discrimination of orientation-

defined texture edges. Vision Research, 35(20), 2863-2877.

Yap, Y.L., Levi, D.M., & Klein, S.A. (1989). Peripheral positional acuity: Retinal and cortical constraints on 2-dot separation discrimination under photopic and scotopic conditions. Vision Research, 29 (7), 789-802.

Yu, C., & Essock, E.A. (1996). Spatial scaling of end-stopped perceptive fields: Differences in neural bases of end-zones, flanks and centers. Vision Research, 36, 3129-3139.

Appendix A: Pretest 1: SC with Constant Stimuli

Method

Participant. One participant voluntered (age = 23). His vision was corrected to normal as judged by his optometrist, and he wore his corrective glasses throughout the testing sessions.

Apparatus. Testing and data collection was done using a Quadra McIntosh equipped with a 640 x 480 pixels color monitor (28 pix/cm, refresh rate = 66.7 Hz).

Stimuli. Stimuli were created using a right oblique sinusoidal grating (45°) within a circular aperture of 3° of diameter (foveally in degrees of visual angle). The wavelength (distance between two peaks) could be varied (1, 2.5, 3, 3.5, 5, 10, 12.5, 15, 25 cpd foveally). In the center of the aperture, the phase was changed by 90° within a rectangular patch of 2:1 dimensions (equivalent to a change of polarity within the rectangular region). To ensure no average luminance difference between the rectangle and the background grating, their centers (sin 0°) were co-aligned with the center of the aperture. Both gratings had their average grey equal to background luminance. The rectangular region could be either vertical or horizontal and was varied in size from 3.75′ to 120′ of arc in sqrt(2) steps.

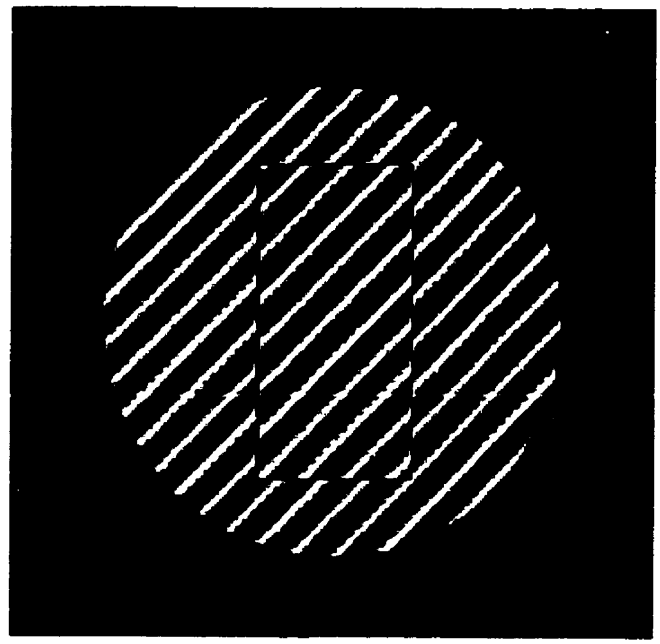

Figure 16. Stimulus example from Pretest 1. The grating's orientation always remained right oblique, but the SC defined rectangle could be vertical or horizontal.

Procedure. The participant foveated a fixation point (a red led) present at all times (except for the foveal condition), placed in the same depth plane. Participants pressed a key to initiate the trial. The stimulus appeared for 45 ms after which it was replaced by a grey area. The participant had to tell the orientation (vertical or horizontal, p = 0.5) of the subjective rectangle in a 2 alternative forced-choice task. Percent correct was collapsed over the two orientations.

The participant was tested for a range of rectangle size and wavelength. Eccentricities tested were foveal (0°), 5°, 10°, 20° and 40°. Because past research reports a temporal visual field preference (Paradiso & Carney, 1988; Rovamo & Virsu, 1979), both temporal and nasal visual fields were tested. Average screen luminance was 32.5 cd/m^2. Viewing distances were set using Equation 10 where E_2 was 5.0° and Df was 200 cm.

Results

Analysis and Model Fitting

Data Selection. For each condition, threshold size and wavelength at 75% correct was found by fitting a logistic function (Figure 17A & 17B). Thresholds in the low range of wavelengths (high ranges of sizes) were obtained by fitting a curve at a fixed size for variable wavelength. To be kept, data points had to fulfill three criteria: (1) the curve had to explain at least 50% of the variance, (2) the threshold had to be within the range of stimuli tested and (3) the slope had to be in the predicted direction. These criteria are liberal, permitting to keep more data points for the purpose of well constraining the fitting functions, with the risk of introducing noise in the data.

Only 6.3% (n=5) of the data points were derived from Weibulls that accounted for 50% to 70% of the variance. These points did not appear anomalous when compared to the other data points. 81.0% of the data points (n=63) originated from curves explaining more than 80% of the variance.

Model. To asses the goodness of fit of a model, a certain number of transformations were done to the data. (1) The data (Figure 17A) are plotted and subsequently used as logs (Figure 17B). (2) The rectangular parabola is fit to the foveal data in the log space (see Equations 5 & 6). (3) A scaling factor for each eccentricity was found that shifted the foveal rectangular parabola to fit the given peripheral data set. (4) Data is plotted after magnification (dividing the ω and s coordinates by the IMF) around the foveal rectangular parabola, both in the normal (see Figure 17C & 17E) and log space (see Figure 17D & 17F), to show how well the model accounts for the data for either the classic method (see Figure 17C & 17D) or the multiple method (see Figure 17E &

17F).

Figure 18 show the recovered scaling factors for each eccentricity. Forcing the line through (0,1), linear fit of scaling as a function of eccentricity permits to measure E_2 (=1/slope). Because visual fields have been reported to be asymmetric in magnification, independent E_2s for each visual field were derived. Figure 18 also show the two E_2s of the multiple method (one for the wavelength and one for the size of the rectangle).

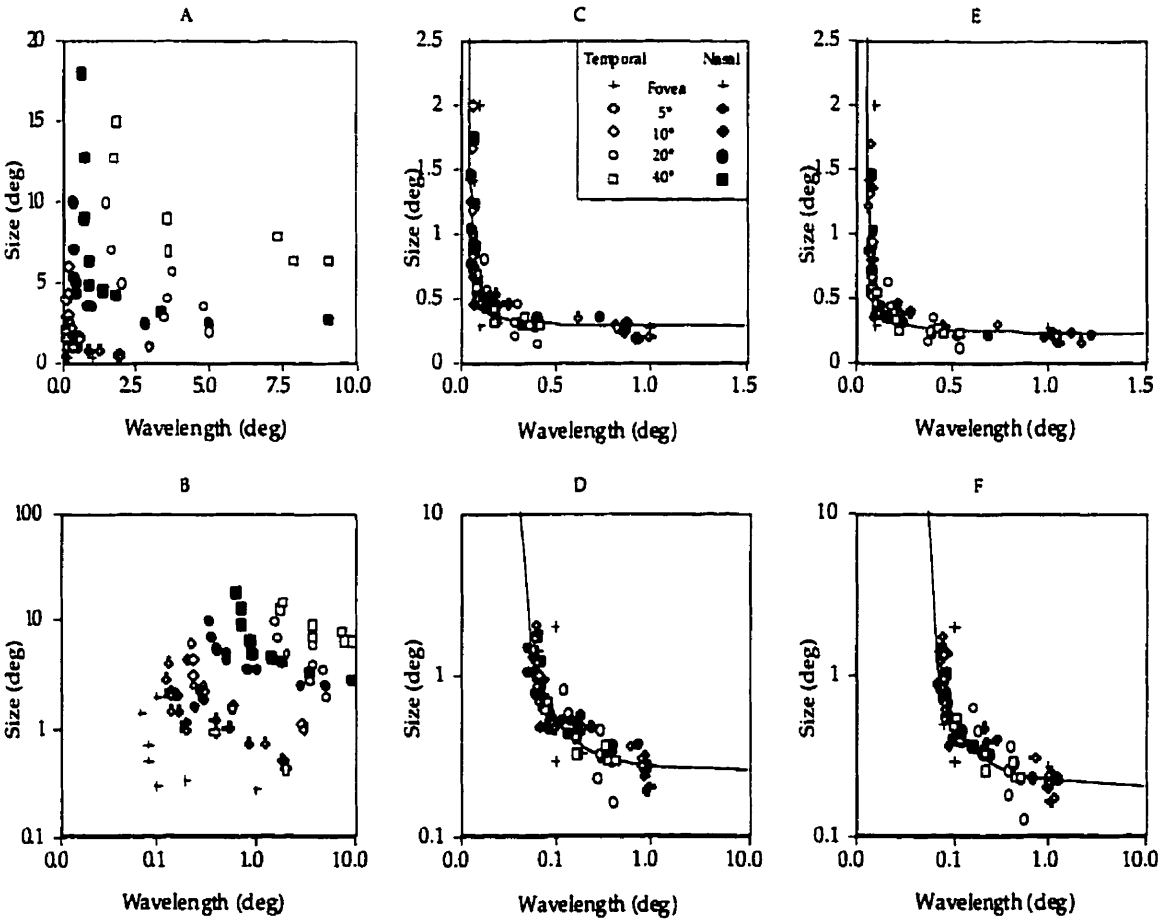

Figure 17. Data of Pretest 1. Panels A, C and E are shown in normal coordinates and B, D and F are in logarithmic coordinates. (A, B) Unmagnified data set. (C, D) Data set after collapsed using scaling factors derived with the "classic" method. (E, F) Same as (D, E) but using scaling factors derived with the "multiple" method. Data are shown for temporal (black symbols) and nasal (white symbols) visual fields.

Explained Variance. Several residual sums of squares were compared

to test the explained variances of different models. Table 9 shows the total variance ("total"; Figure 19A), the variance around the mean at each eccentricity ("eccentricity"; Figure 189), the variance accounted for by the use of magnification and the parabola ("model"; Figure 19C) and the variance derived when the parabola derived by the model is placed at an eccentricity where it can account for the maximum variance ("parabola"; Figure 19D). This last step was done to compare the model with the use of the parabola by itself.

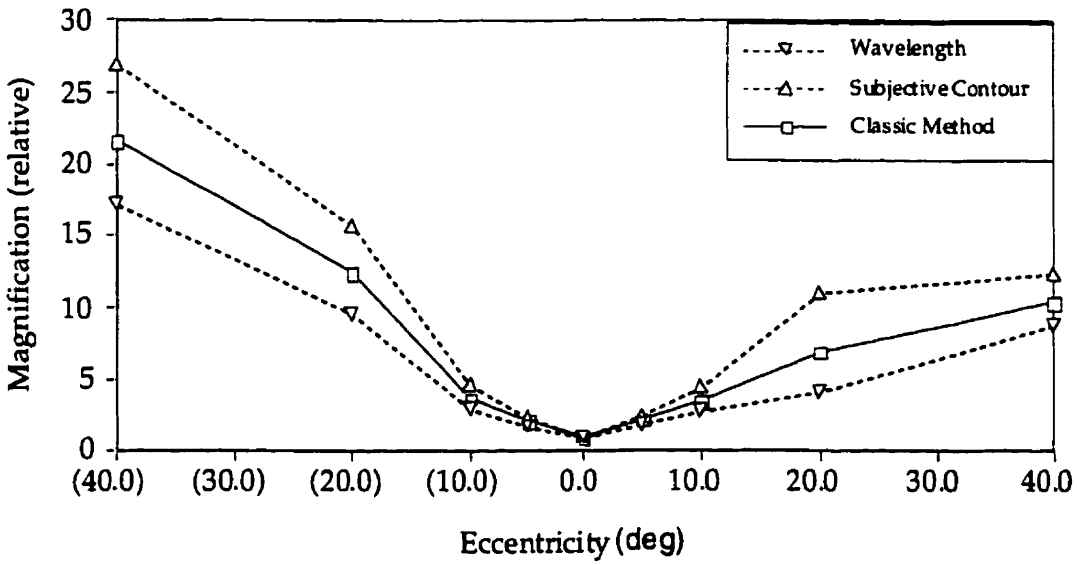

Figure 18. Scaling factors of Pretest 1. Eccentricities in parentheses are from the nasal visual field (temporal retina). The classic method (squares) recovered scaling factors that were always between scaling factors recovered by the multiple method (triangles), which recovered larger scaling factors for the SC length (upwards triangles) than for the wavelength (downwards triangles). Also, an asymmetry of visual field was observed, the nasal visual field (temporal retina) requiring larger scaling for equal performance to occur.

Table 9: Variance and Residuals in Pretest 1

Model		df	SS	R^2	R^2_{adj}	t	p
	Total	78	9.523				
	Eccentricity	70	.513	94.6	94.0	55.70	<.0005
Classic	Parabola	76	12.569	—	—	—	—
	Model	74	3.411	64.2	60.1	17.27	<.0005
Multiple	Parabola	76	8.753	8.1	—	—	—
	Model	72	1.658	82.6	80.6	28.69	<.0005

note: — is used to denote impossible values (for example: negative R^2_{adj}).

For both models, the parabola doesn't improve predictability of scores by itself. Moreover, the eccentricity-dependent variance wasn't all accounted for. It should be noted that instead of using the actual IMFs derived for each eccentricity in order to estimate the residuals, the predicted IMFs from the E_2 derived was used. This has the effect of increasing the residuals. Nevertheless, these two models accounted for 64.2% (classic) and 82.6% (multiple) of the total variance (ps < .0005), the multiple model accounted for 51.4% of the variance not accounted for by the classic model ($t = 14.47$, $p < .0005$). Therefore, the multiple model is considerably more accurate than the classic model.

Classic vs Multiple: An Examination of E_2s

The multiple method gave consistently higher scaling factors for the size parameter than for the wavelength parameter ($p < 0.004$). The classic method would predict no difference between the two magnifications except for random noise. Table 10 presents for each method the E_2 recovered, the correlation between scaling and ecentricity and a test of significance of slope (t). These values are presented for both the temporal and nasal retina. The last column of Table 10 presents a test of the difference of E_2 between the temporal and nasal retina. The last three rows of Table 10 presents the same test applied to differences between fitting techniques. Statistical tests for the slope difference were used to test E_2s (=1/slope) and the difference between E_2s. All IMFs were significant (see Table 10). Moreover, the slope of the size IMF was steeper (smaller E_2) than the slope for the wavelength IMF for both the temporal and nasal retina. However, only the nasal wavelength IMF differed significantly from the classic prediction. This is not surprising because the classic predictions were between the size and wavelength predictions of the

multiple method. Predictions for the classic method followed the magnifications for the size and wavelength. However, our results show that these are systematically different hence should be estimated and subsequently scaled seperately. Also, a visual field effect was observed for the classic and multiple, both for wavelength and for size IMFs, the temporal retina having a steeper IMF.

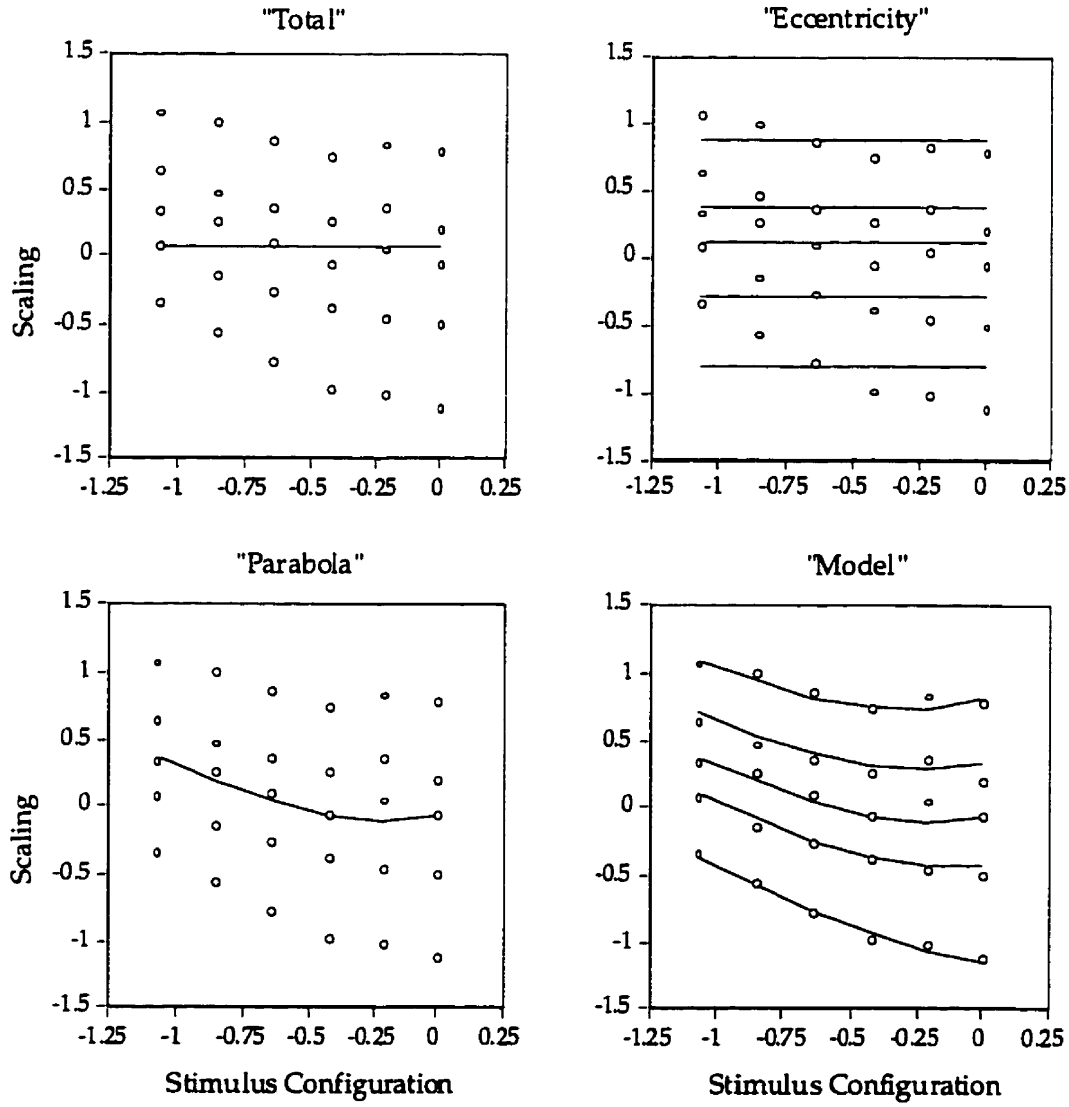

Figure 19. Calculation of residuals. Residuals were calculated adding the distance between the data and the line for the same eccentricity. (A) Total variability refers to variability compared to the mean of all data. (B) Eccentricity variability refers to variability as compared to the mean of data seperately for each eccentricity. (C) Parabola variability refers to the fit when only one parabola is used to fit the data. (D) Model variability refers to when

variability is fit by a rectangular parabola which is scale for eccentricity. The data set shown comes from Pretest 2.

Table 10: E_2s for Temporal and Nasal Retinas

method	Temporal			Nasal			t (diff)
	E2	r	t	E2	r	t	
classic	2.121	0.986	8.405***	4.022	0.974	12.31****	3.322††
mult. wav.	2.758	0.990	7.990***	5.598	0.972	14.06****	3.354††
mult. size	1.654	0.879	8.795****	2.868	0.976	04.08**	2.402†
class. vs wav.			1.305				2.969†
class. vs size			1.320				1.327
wav. vs size			2.570†				2.294†

one-tail slope t-tests (4 d*f*): ****p≤.001, ***p≤.005, **p≤.01, *p≤.05
one-tail slope paired t-tests (6 d*f*): ††p≤.01, †p≤.05

Visual Acuity. The minimum wavelength (ω_{min}), size (s_{min}) and the eta (ξ) values were 2.67′, 1.46′ and 7.95′ for the classic method and 3.38′, 12.01′ and 7.65′ for the multiple method. There seems to be a fair agreement between the different methods except for the E_2 values.

Discussion

Although the multiple method finds that scaling for size is larger than for wavelength, these predictions can be approximated with a lower degree of accuracy by the classic method. However, systematic differences between MFs and between E_2s indicate that this effect cannot be disregarded on the basis that data seem to overlap well using one E_2. A complete explanation of SCs require at least two E_2s.

The visual field effects were replicated for both the classic and multiple model. In the case of the multiple model, both size and wavelength showed a visual field asymmetry, suggesting that both stages processed preferably the temporal visual field. If a visual field preference existed only at the retinal ganglion cell level (Rovamo & Virsu, 1979), it wouldn't normally show up in both size and wavelength E_2s. It seems more likely that the same asymmetry is present throughout SC encoding.

Appendix B: Pretest 2: SCs with Threshold Estimation

The sampling strategy described in the "Prediction and Error from Prediction" section was used.

Method

Participant. The same participant as in pretest 1 voluntered.

Apparatus. The same apparatus as in experiment 1 was used.

Stimuli. SCs were constructed using two perpendicular gratings, as shown in Figure 20. The rectangle's corners always fell on black spots of the composite grating except for the lowest wavelength case, where the corners fells equally on white and black spots.

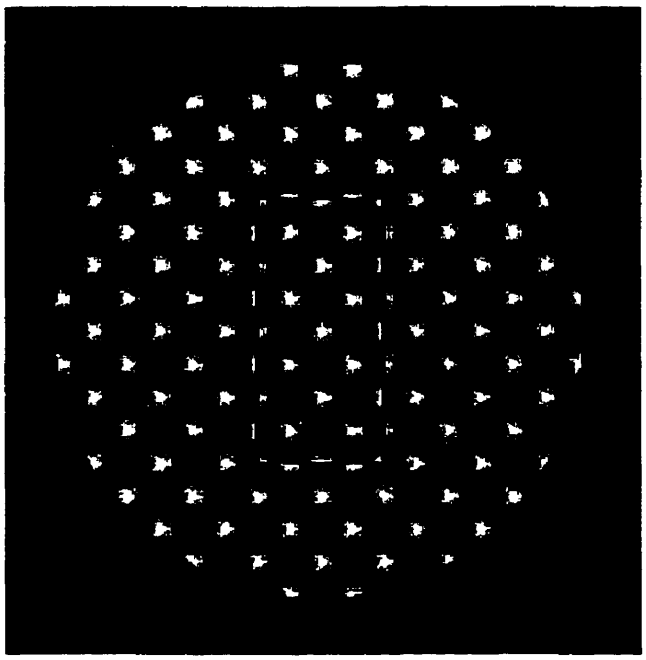

Figure 20. Stimulus of Pretest 2. The texture was created by adding two diagonal orthogonal gratings. The distance between two vertical or two horizontal white points is sqrt(2) of the wavelength of the gratings.

Procedure. The same procedure as in experiment 1 was used, except that a modified BEST-PEST was used (Lieberman & Pentland, 1982). The BEST-PEST controlled the scaling of the stimuli. The ratio of cycles per rectangle's length varied from condition to condition from 1 to 32 cycles per SC length in steps of 2 (one wavelength of the composite grating being sqrt(2) the wavelength of the underlying gratings). Foveal viewing distance was 100 cm and distances for more eccentric viewing distances were set using an E_2 of 2.5° [see Equation 10]. Presentations were in the temporal retina (nasal visual field).

Results

Analysis and Explained Variance.

Results for the two methods are shown in Table 11 and Figure 21A. The same method presented in Pretest 1 was used to derive the sums of squares (SS) in Table 11. The eccentricity variable alone accounted for 90.6% of the total variance. The addition of the parabola with one or two magnifications accounted for almost all of the variance. However, with such high R^2, statistical tests of the R^2 increase are not recommended because they are inaccurate (Hays, 1970).

Table 11: Results of Experiment 2

Model		*df*	SS	R^2_{adj}	t	p
	Total	29	10.843			
	Eccentricity	25	1.024	89.1	15.49	<.0005
Classic	Parabola	27	9.972	1.2	1.54	>.10
	Model	26	.221	97.8	35.32	<.0005
Multiple	Parabola	27	9.985	1.1	1.52	>.10
	Model	25	.137	98.5	45.01	<.0005

Classic vs Multiple: Local Y Slope Change

Because the regression lines were fixed, a difference between E_2 test as used in Pretest 1 couldn't be performed. An alternative method of testing the difference between the two theories is to test the change in slope of scaling as a function of configuration. This slope should be constant according to the classic method but should gradually change with eccentricity according to the multiple method. Table 12 presents the characteristics of the relationship between scaling and configuration (slope, intercept, variance accounted for and statistical test) and the slope change test applied to slope differing by 1, 2, 3 or 4 levels of eccentricity (for example, t Δ2 at eccentricity of 2.5° reports the t-test between the slope for eccentricities of 2.5° and 10°). The multiple method was supported by a gradual change in slope with eccentricity, the larger the eccentricity difference the larger the slope difference. There was a difference in slope between the foveal and 20° of eccentricity. This indicates a *configuration shift* as well as a scaling shift (see Equations 4 & 7). In terms of SC length and wavelength, it indicates that SC length and wavelength don't magnify at the same rate.

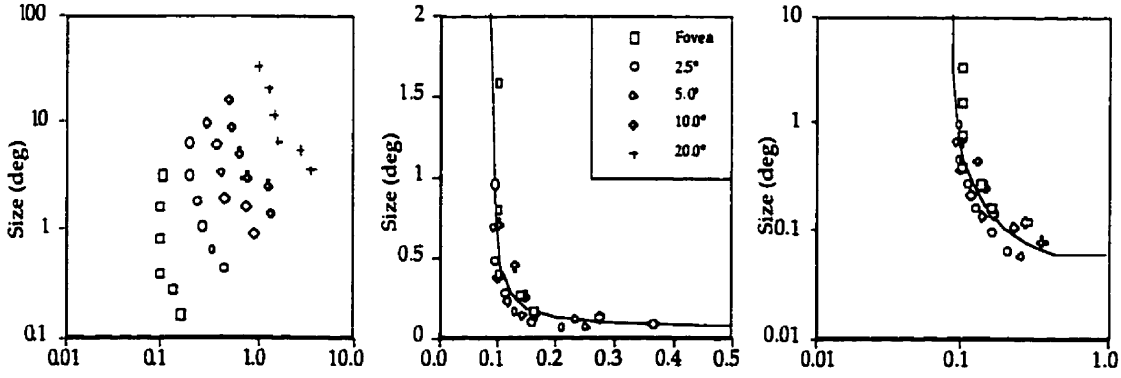

Figure 21. Data of Pretest 2. (A) Unmagnified data in logarithmic space. Using the IMFs derived with the "multiple" method, the data was collapsed (B: normal coordinates, C: logarithmic coordinates). Also shown is how well the data was fit by the model (line in B and C). In (A), a change of slope is apparent. This change of slope points to the inability of one IMF to account for all types of vairability in the data associated with eccentricity.

Table 12: Slope Change

Ecc.	Characteristics				Slope Change			
	Slope	Intercept	R^2	t(4)	t Δ1	t Δ2	t Δ3	t Δ4
0	-.7325	-1.192	.945	-8.313***	1.79	3.04††	3.05††	3.74†††
2.5	-.5354	-.5651	.942	-8.806***	1.63	1.65	2.42†	
5	-.3594	-.0864	.816	-4.219**	.030	0.69		
10	-.3558	.1920	.810	-4.125**	.659			
20	-.2763	.7329	.729	-3.283*				

one-tail slope t-tests (4 d*f*): ***p≤.005, **p≤.01, *p≤.05
one-tail slope paired t-tests (6 d*f*): †††p≤.005, ††p≤.01, †p≤.05

Visual Acuity. The foveal visual acuity for the gratings for classic and multiple methods were 15.86 and 20.76 cpd respectively (11.22 and 14.68 cpd for the individual gratings) which equals 2.89′ and 3.78′ arc (4.09′ and 5.35′ arc for individual gratings). The acuity for rectangle was about 3.75′ and 2.10′ arc. Values of ξ were 7.83′ and 5.25′ respectively.

Discussion

The variance accounted for by the models were much higher than in the first pretest. This increase in explained variance may be due to several factors: practice, better sampling method and all testing for an eccentricity was done in one session.

As expected, findings from the first experiment were replicated despite the changes in methodology. The use of an IMF reduced the variance associated with eccentricity in both the normal (Figure 21B) and the log space (Figure 21C). Moreover, using the rotated logs transform (see Equations 4 & 5), the systematic slope change with eccentricity becomes apparent (Figure 19). The significant change in slope between eccentricities is predicted by the multiple method but not by the classic method.